103

Modeling of Ultrasonic Processing

by

Wenguang Zhao

Submitted to the Department of Civil and Environmental Engineering
in partial fulfillment of the requirements for the degree of

Master of Science

at the

MASSACHUSETTS INSTITUTE OF TECHNOLOGY

September 2005

Signature of Author .....
Wenguang Zhao
Department of Civil and Environmental Engienering
August 12, 2005

Certified by .....
David Roylance
Professor, Department of Materials Science and Engineering
Thesis Supervisor

Certified by .....
Jerome J. Connor
Professor, Department of Civil and Environmental Engineering
Thesis Reader

Accepted by .....
Andrew Whittle
Professor, Department of Civil and Environmental Engineering
Chairman, Department Committee on Graduate Studies

Modeling of Ultrasonic Processing

by

Wenguang Zhao

Submitted to the Department of Civil and Environmental Engineering
on August 12, 2005
in partial fulfillment of the requirements for the degree of Master of Science

Abstract

This paper presents a finite element analysis (FEA) of ultrasonic processing of an aerospace-grade carbon-epoxy composite laminate. An ultrasonic (approximately 30 kHz) loading horn is applied to a small region at the laminate surface, which produces a spatially nonuniform strain energy field within the material. A fraction of this strain energy is dissipated during each ultrasonic loading cycle depending on the temperature-dependent viscoelastic response of the material. This dissipation produces a rapid heating, yielding temperature increases over $100^{\circ}C$ in approximately 1s and permitting the laminate to be consolidated prior to full curing in an autoclave or other equipment. The spatially nonuniform, nonlinear, and coupled nature of this process, along with the large number of experimental parameters, makes trial-and-error analysis of the process intractable, and the FEA approach is valuable in process development and optimization.

Thesis Supervisor: David Roylance
Title: Professor of Materials Science and Engineering

Thesis Reader: Jerome J. Connor
Title: Professor of Civil and Environmental Engineering

ACKNOWLEDGEMENTS

I would like to express my sincere gratitude to my thesis advisor, Professor David Roylance for introducing me to the field of finite element modeling of ultrasonic processing. I met Professor Roylance at the most difficult time in my academic career. Without out his support, I would not be able to find a way out. He had time and time again helped me with encouragements and invaluable advice. His tolerance and patience throughout the course of this study is most appreciated. This work would not have been completed without his guidance. He has been a good advisor, a good teacher, and a good friend. I enjoyed very much sharing his interesting stories and American culture.

I want to acknowledge the Motorola MUST/MIT program for their financial support of this work, which made this thesis in reality.

I would like to express my great appreciation to Professor Shi-Chang Wooh for his help on my admission to MIT. His decision changed my whole life. It was such a pity that he had to leave and I could not work with him. I wish him all the best in his own career.

I want to thank Professor Jerome J. Connor for his kindness to help on the thesis reading. The discussion with him about the application of composites on Aeronautical engineering was very interesting. Thanks for his precious time.

I want to thank Professor Daniele Veneziano and Professor Oral Buyukozturk for their kindest support and direction.

I also wish to thank John Player, for his generous help and making available the experimental data and the sources of his research.

I would finally like to thank my parents for their love and sacrifices; and my wife for her endless encouragement and tolerance.

Table of Contents

List of Figures

List of Tables

Chapter 1

Introduction

This thesis explores the consolidation stage in the curing process of thermoset-resin fiber-reinforced composites, in which heating is produced by viscoelastic dissipation arising from oscillatory loading. Curing is the polymerization (crosslinking) of the resin matrix to create a permanent bond between the fibers and between the individual lamina. Normally, the curing process is accomplished by exposing the material to certain temperatures and pressures for a predetermined length of time. The curing of thermosetting resins is an exothermic reaction and requires elevate temperature to accelerate the crosslinking reaction. The temperature depends not only on the amount of heating power supplied but also on the rates of thermal conduction inside the materials and convection from its surface. Hydrostatic pressure is also needed to squeeze excess resin out of the composites, to consolidate the individual plies, and to decrease the formation of voids. The magnitude and duration of the temperatures and pressures applied during the cure cycle has a significant effect on the quality of the finished part.

In most cases the typical cure cycle is composed of two steps. The first step is called the consolidation stage. In this stage, the viscosity of the resin is reduced by heating to an intermediate temperature. Pressure or vacuum is applied to squeeze the excess resin from the laminate and to consolidate the individual plies together. Prepreg consolidation is one of the most important steps during composite preparation. If prepregs are not well consolidated, air bubbles may be trapped within the final products. This may affect the mechanical properties of the cured composites.

The second step is called the cure stage. In this stage, the temperature is increased further to initiate the polymerization of the resin. This temperature is maintained until the polymerization is complete. The material is then cooled down. This thesis focuses on the consolidation stage and does not include the cure reaction.

An autoclave is most widely used to consolidate prepregs of composite materials [1]. It offers enhanced processing flexibility compared to other common processing equipment such as an oven or press. However, composite processing by autoclave is very costly in terms of capital investment, and limits the size of the parts that can be produced. To address this issue, many researchers have emphasized the development of out-of-autoclave processing techniques for high temperature resistant composites.

A non-autoclave vacuum bag process alone is an alternative for autoclave processing [2]. This type of process utilizes atmospheric pressure created by the vacuum bag alone, and eliminates the need for external pressure normally supplied by an autoclave. Hence, it does not require large capital expenditures for tooling and processing equipment, and is cost effective for composite processing. However, the vacuum application point has to be carefully selected to achieve the final consolidated laminate net shape and resin content without excessive resin squeeze-out.

In this thesis, comparing with the autoclave and vacuum debulking, another interesting alternative is proposed as ultrasonic debulking followed by baking in an oven, which is called ultrasonic tape lamination (UTL).

1.1 Problem Statement

1.1.1 Ultrasonic Processing

UTL is a technique in which a probe tip oscillating at ultrasonic frequency of 20-40 KHz is applied to the surface of the uncured part to cause a cyclic indentation. A fraction of the induced strain energy is dissipated as heat due to the material's viscoelastic properties. This also generates the pressure needed for the consolidation stage in the cure cycle.

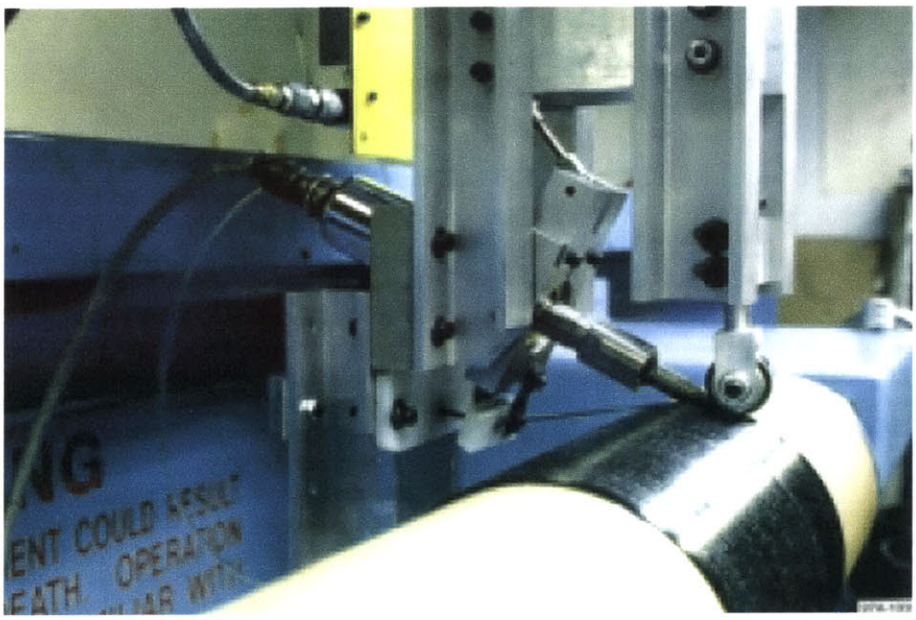

Figure 1. Ultrasonic tape lamination during filament winding (Roylance, 2004)

Although ultrasonic welding or turning have been widely used in industries, ultrasonic processing for consolidation purpose has only been investigated and implemented in recent years. Figure 1 shows the ultrasonic tape lamination process during filament winding. In order to avoid damaging the composites, suitable ultrasonic

horn amplitude and horn angle are required. The applied amplitude and horn angle change the stress and strain states in the laminates and thus changes the dissipated energy during viscoelastic heating. The amplitude should provide sufficient energy level for resin flow and penetration depth. The range of the amplitude for UTL is between 15 and 60 microns. The horn angle applied changes the contact area and pressure. To provide a good support for consolidation, a normal contact load is between 1 and 10 pounds. During UTL process, a horn angle of less than 90^{o} is required to achieve balanced energy input and suitable pressure to have coupling with adequate compaction.

The effects of amplitude and pressure of the ultrasonic horn during UTL have been investigated by Roylance et al [3]. Their research indicated that the viscoelastic heating dominates the UTL heat generation in the polymer prepreg and the contact pressure has no obvious effect. Tolunay et al. [4] also found that the viscoelastic heating occurs over the whole volume of soft polymer during ultrasonic welding and the interface did not have a significant effect on the amount of heat dissipated. Based on these results, though the real UTL process combines viscoelastic and frictional heating, our model only considers viscoelastic energy dissipation as volumetric heat sources rather than frictional heating at the interfaces.

1.1.2 Numerical Simulation

The whole UTL process is very complex. This is mainly because there are plenty of experimental parameters, such as ultrasonic horn angle, oscillation amplitude, frequency, density, specific heat, and others, which makes the physical experiments expensive, difficult, and time-consuming. Such studies can be performed effectively by numerical

simulation. Mathematical modeling is very useful and powerful in optimizing these processing operations. For such a nonisothermal problem, the governing equations are the well-known conservation equations for transport momentum and energy. These equations can be solved in several ways, including finite difference analysis and finite element analysis.

Finite element analysis for such a heat transfer problems is the subject of this thesis. Finite element modeling can help us to understand the thermo-mechanical coupling on the deformation behavior in complicated processing situations where many factors have to be taken into account. It can also provide an insight into the effects of temperature sensitivities. More important, it helps to find the optimal setting of the experimental parameters for UTL.

In the literature of numerical simulations of processing as well as transient heat transfer for polymer composites, both finite element method and finite difference method are utilized broadly. Thus, they are introduced briefly as follows:

Pusatcioglu et al. investigated the temperature gradient developed during the casting of unsaturated polyester by solving the one-dimensional heat transfer equation using experimentally determined reaction kinetics and thermal conductivities [5]. Lee and Springer presented a one-dimensional analytical cure model for prepreg composites. A finite-difference cure-modeling program based on this model uses implicit method to calculate the degree of cure and, it can also analyze the tool and the bagging [6].

Roylance et al. used finite element analysis in modeling the processing of composite materials. His paper demonstrated interesting applications of finite element codes to solve the equations governing non-isothermal, reactive, and transient viscous

flow processes. A time-stepping algorithm was used to model pultrusion processing, fabric impact and ultrasonic processing [7, 8, 9].

Bogetti and Gillespie studied two-dimensional anisotropic cure simulations of thick thermosetting composites using boundary fitted co-ordinate systems with the finite-difference technique. The solution was reported to be mesh-dependent [10]. Young investigated the resin-transfer moulding process and developed a six-node wedge element to model the non-isothermal mould filling [11].

Loos and Springer developed a one-dimensional finite difference model to simulate the cure process of a flat plate [12]. Based on their finite difference modeling, Loos and MacRae followed to develop a two-dimensional finite element model to simulate the resin film infusion process including curing [13].

Yi et al. developed a nonlinear transient heat transfer FE model to simulate the curing process of polymer matrix composites. Temperature field inside the laminates was evaluated by solving the nonlinear anisotropic heat conduction equations including internal heat generation produced by exothermic chemical reactions [14].

Joshi et al. used a general-purpose FE package for cure modeling. Application of transient heat-transfer analysis is demonstrated by modeling the cure of thick prepreg laminate, a honeycomb sandwich panel and an I-beam. Stability with respect to the FE density and the length of the time step employed is also investigated [15].

Different researchers have developed different-purpose numerical software to study the processing of composites. We used a code adapted from the Zienkiewicz text [16] with a special element developed by Roylance et al. to model the nonisothermal processing operations for fiber-reinforced thermoset polymer composites. The theoretical

background and numerical implementation of the procedure are described. Because the curing temperature of the studied carbon/epoxy prepreg is $350\,^{\circ}F$ ($177\,^{\circ}C$) and the temperature fields in the UTL simulations are below $150\,^{\circ}C$, the cure reaction is not included. We only considered the consolidation stage of the laminates due to the viscoelastic dissipation without considering the internal heat generation produced by exothermic chemical reactions

1.2 Objectives of the Research

The general objective of our research is to develop both the computational and the experimental bases for the ultrasonic processing of fiber-reinforced thermoset polymer composites. Specifically, the purpose of this work is to develop a process model for the optimization of UTL experimental parameters. The overall research consists of the following tasks:

1. To carry out material characterization of a practical epoxy resin to obtain parameters for numerical simulations;
2. To extend and verify finite element analysis (FEA) codes and compare the computational results with the experimental results.

It is expected that the results of this work will form a basis for further advancement of UTL experimental optimization and the development of an effective control system for material engineering applications.

1.3 Research Approach

Material characterization is performed using techniques including Fourier Transform Infrared Spectroscopy (FTIR), Differential Scanning Calorimetry (DSC), Dynamic Mechanical Analysis (DMA), and Thermogravimetric Analysis (TGA). FTIR was used for the identification of the given epoxy resin. Uncured, partially-cured and fully-cured samples were used for FTIR to investigate the cure mechanism. Both DSC and TGA were used to explore the thermal behavior of the given epoxy resin at high temperatures. The glass transition temperature and fiber weight fraction were obtained from these tests. DMA was also used to analyze the viscoelastic response of the samples. The results were compared with those of the previous research. The viscoelastic constants of a similar epoxy resin based on DMA tests were then decided to use for our simulation.

These characterized material parameters are used as inputs for numerical simulation. The viscoelastic heat dissipation is simulated by a FEA code adapted from Zienkiewcz's text. The source code is written in FORTRAN. The element in the FEA code models the governing equations for polymer processing, which are the governing equations for transient heat transfer. This special element developed by Roylance et al. [9] has the capability to couple the mechanical and thermal fields. The output of this simulation is the stresses, strains and temperature fields at different time steps. It can demonstrate the mechanical and thermal evolution inside the laminates.

To validate the simulated results, static UTL experiments were performed by Foster-Miller Corporation. The temperature picked up of the computational and experimental results showed an acceptable match. A comparison with the analytical solution for the displacement fields was also implemented for the 2-D case.

A more functional and powerful post-processor was developed for the FEA code to plot the 2-D images of the computational results. A graphical interface was also developed using MATLAB to create the animated movie of the mechanical and thermal evolution inside the laminates.

Chapter 2

Theoretical background

2.1 Governing Equations

In such thermo-mechanical coupled heat conductions, the dynamic or transient field problems lead to a set of differential equations governing the nonisothermal flow. The energy equation governing the heat transfer is:

$$\rho c \frac{\partial T}{\partial t} = Q + \nabla(k \nabla T) \tag{1}$$

where ρ is density, c is specific heat, Q is heat generation rate, and k is thermal conductivity. It is assumed that the fiber and resin form a homogeneous system and are at the same temperature during the simulation process.

To formulate the governing equation of the transient heat conduction problem in equation (1) using Galerkin method, we proceed on the finite element discretization based on the assumption of a trial function expansion

$$T = \Sigma N_i \phi_i = N\phi \tag{2}$$

where N_i are shape functions prescribed in term of independent variables, ϕ is the nodal temperature vector. For the transient case, assembly of elemental contributions results in the global system equations in the form of [16]

$$C\dot{\phi} + K\phi + p = 0 \tag{3}$$

where

$$C = \int_{\Omega} N^T \rho c N d\Omega$$

$$K = \int_{\Omega} \nabla^T N k \nabla N d\Omega \tag{4}$$

$$p = \int_{\Omega} N Q d\Omega$$

Similarly, the governing equation of displacement is

$$L^T D L u = 0 \tag{5}$$

where L is a suitable linear operator and D is an elasticity matrix containing the appropriate properties.

If we proceed on the finite element discretization on the displacements

$$u = \Sigma N_i a_i = Na \tag{6}$$

where a is the nodal displacement vector. Assembly of elemental contributions results in the global system equations in the form of [16]

$$Ha = f \tag{7}$$

where $B = LN$ and

$$H = \int_{\Omega} B^T D B d\Omega \tag{8}$$

$$f = \int_{\Omega} B^T \sigma d\Omega$$

2.2 Viscoelastic Heat Generation

A viscoelastic material under cyclic loading will dissipate a fraction of energy as heat. The heat generation rate Q in equation (1) can be obtained from linear viscoelasticity

[17]. If we assume that the material is subjected to a sinusoidal strain, the heat generation rate is given by:

$$Q = f \cdot W_{dis} = f \cdot \frac{E''}{E'} \cdot W_{st} \tag{9}$$

where f is the frequency, W_{dis} is the net dissipation per cycle, and W_{st} is the maximum stored energy per cycle. E' is the real modulus and E'' is the loss modulus. These viscoelastic moduli can be obtained from Wiechert model in linear viscoelasticity as

$$E' = k_0 + \sum_{j=1}^{N} \frac{k_j (\omega\tau_j)^2}{1 + (\omega\tau_j)^2}$$

$$E'' = \sum_{j=1}^{N} \frac{k_j (\omega\tau_j)}{1 + (\omega\tau_j)^2} \tag{10}$$

where k is spring stiffness and τ is relaxation time for each element in Wiechert model. Temperature has a dramatic influence on rates of viscoelastic response. For thermo-rheologically simple materials, the temperature dependence can be introduced by assuming that the relaxation times τ's obey an Arrhenius relation of the form:

$$\tau_j = \tau_{0j} \exp\left(\frac{E^\tau}{R_g T}\right) \tag{11}$$

Where the τ_{0j} are the preexponential constants, E^τ is an activation energy for visco-elsticity and R_g is the gas constant. Each τ_j is given the same activation energy. Numerical parameters τ_{0j}, k_j and E^τ for this model have been obtained by means of dynamic mechanical analysis (DMA).

2.3 Finite Element Formulation

We use two-point recurrence schemes to solve the first order equations in (3), we assume:

$$\begin{aligned} \phi &= N_n \phi_n + N_{n+1} \phi_{n+1} \\ \dot{\phi} &= \dot{N} \phi_n + \dot{N}_{n+1} \phi_{n+1} \end{aligned} \tag{12}$$

Noting that a time interval Δt exists with N_i taking the values N_n and N_{n+1}. We substitute (12) into (3) and obtain [16]

$$\left(\frac{C}{\Delta t} + K\theta\right)\phi_{n+1} + \left(-\frac{C}{\Delta t} + K(1-\theta)\right)\phi_n + p = 0 \tag{13}$$

For Galerkin method, θ factor equals 2/3.

From equation (13), we can obtain

$$\left(\frac{C}{\Delta t} - \theta K\right)\Delta\phi = p - K\phi_n \tag{14}$$

where inside the elment,

$$C_{jk}^e = \int_{\Omega^e} N_j \rho c N_k d\Omega$$

$$p_k = \int_{\Omega^e} N_k Q d\Omega$$

$$K_{jk}^e = \int_{\Omega^e} \nabla^T N_j k \nabla N_k d\Omega$$

$$= \int_{\Omega^e} \left(\frac{\partial N_j}{\partial x} k_x \frac{\partial N_k}{\partial x} + \frac{\partial N_j}{\partial y} k_y \frac{\partial N_k}{\partial y} \right) d\Omega$$

$$K^e_{jk} \cdot \phi_n = \int_{\Omega^e} \left(\nabla^T N_j k \nabla N_k \right) d\Omega \cdot \phi_n$$

$$= \int_{\Omega^e} \left(\nabla^T N_j k \nabla \phi \right) d\Omega$$

$$= \int_{\Omega^e} \left(\frac{\partial N_j}{\partial x} k_x \frac{\partial T}{\partial x} + \frac{\partial N_j}{\partial y} k_y \frac{\partial T}{\partial y} \right) d\Omega \tag{15}$$

All these terms were coded in the subroutine **elmt03.for**. If ϕ_n and p are known, ϕ_{n+1} can be easily calculated from the above equation (14).

To formulate the governing equation for the displacements, from the Zienkiewicz text [16], we have

$$L = \begin{bmatrix} \frac{\partial}{\partial x} & 0 \\ 0 & \frac{\partial}{\partial y} \\ \frac{\partial}{\partial y} & \frac{\partial}{\partial x} \end{bmatrix} \tag{16}$$

and

$$B = LN = \begin{bmatrix} \frac{\partial N}{\partial x} & 0 \\ 0 & \frac{\partial N}{\partial y} \\ \frac{\partial N}{\partial y} & \frac{\partial N}{\partial x} \end{bmatrix} \tag{17}$$

For plane strain case,

$$D = \begin{bmatrix} D_{11} & D_{12} & 0 \\ D_{21} & D_{22} & 0 \\ 0 & 0 & D_{33} \end{bmatrix} \tag{18}$$

For the transversely isotropic case we considered for the composite case, this elasticity matrix becomes

$$D=\frac{E_2}{(1+\nu_1)(1-\nu_1-2n\nu_2^2)}\begin{bmatrix} n(1-\nu_2^2) & n\nu_2(1+\nu_1) & 0 \\ n\nu_2(1+\nu_1)(1-\nu_1^2) & (1-\nu_2^2) & 0 \\ 0 & 0 & m(1+\nu_1)(1-\nu_1-2n\nu_2^2) \end{bmatrix} \quad (19)$$

where E_1, G_1, ν_1 are associated with the behavior in the plane of the strata and E_2, G_2, ν_2 with a direction normal to these. We also take

$$\frac{E_1}{E_2}=n \quad \text{and} \quad \frac{G_2}{E_2}=m \quad (20)$$

Since $H=\int_\Omega B^T DB d\Omega$, inside the element, we have

$$H^e_{jk}=\int_{\Omega^e} B_j^T DB_k d\Omega \quad (21)$$

where

$$B_j^T DB_k=\begin{bmatrix} N_{j,x}D_{11}N_{k,x}+N_{j,y}D_{33}N_{k,y} & N_{j,x}D_{12}N_{k,y}+N_{j,y}D_{33}N_{k,x} \\ N_{j,y}D_{12}N_{k,x}+N_{j,x}D_{33}N_{k,y} & N_{j,y}D_{22}N_{k,y}+N_{j,x}D_{33}N_{k,x} \end{bmatrix} \quad (22)$$

We also have $f_k=\int_\Omega B_k^T \sigma d\Omega$, where

$$B_k^T\sigma=\begin{bmatrix} N_{k,x}\sigma_1+N_{k,y}\tau_{12} \\ N_{k,y}\sigma_2+N_{k,x}\tau_{12} \end{bmatrix} \quad (23)$$

All these terms were also coded in the subroutine **elmt03.for**.

Chapter 3

Material Characterization

3.1 Carbon/Epoxy Composites

The high performance composites used in modern aerospace industry are composed mainly of fiber-reinforced polymer-matrix composites. They include thermoset (epoxy, polyester, polyamide) or thermoplastic (polysulfone) resins with carbon, glass, aramid, or boron fibers. These fibers can be continuous or discontinuous.

The fibers can be aligned in one direction or woven in two or three-directions. Prepreg is usually supplied in one of the two forms: unidirectional tape, or woven fabric. Unidirectional tapes have fibers running continuously in the lengthwise direction of the roll. Woven fabric prepreg has fibers in the lengthwise and transverse directions. The fiber architecture in unidirectional tape and woven fabric prepreg is shown in Fig. 2.

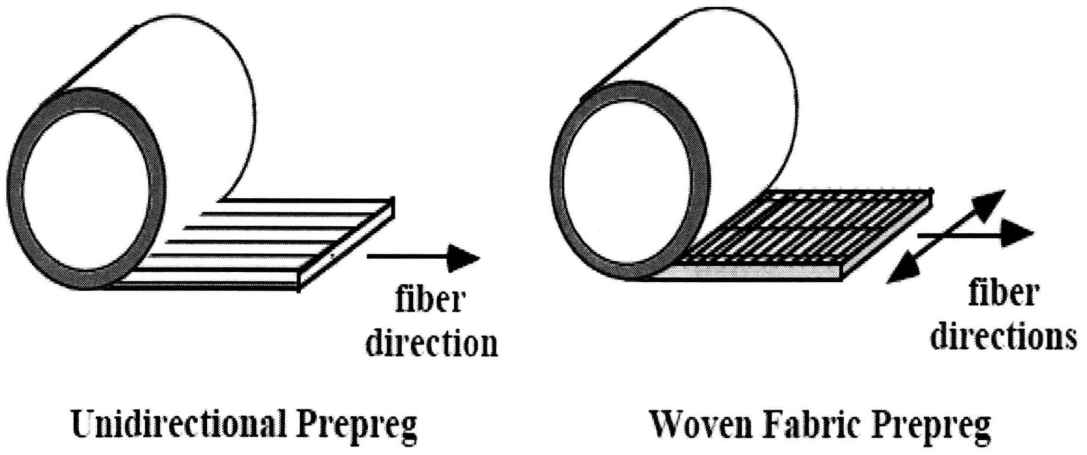

Figure 2. Fiber architecture in unidirectional and woven fabric prepreg (I. M. Daniel, 1994)

The studied material in this project was CYCOM 977-3, a popular high-performance carbon-epoxy composite intended for military and other demanding aerospace applications. More than 95% of thermoset composite parts are based on epoxy and polyester resins. Epoxies have outstanding adhesive properties and are widely used in laminated structures. Though polymer matrix composites based on epoxy resins are used primarily in relatively low temperature applications, carbon fibers have unique properties of high strength at high temperature coupled with low thermal expansion and low density. The outstanding design properties of carbon fiber/epoxy resin matrix composites are their light weight, high strength and modulus, and excellent fatigue performance. With proper selection and placement of fibers, the composites can be stronger and stiffer than equivalent thickness steel parts and weigh 40 to 70% less.

3.2 Epoxy Characterization

3.2.1 Chemical Structure

It is commonly stated in the composite community that CYCOM 977-3 is probably a thermoplastic-toughened TGMDA/DDS (tetraglycidyl methylene dianiline/diamino-diphenyl sulfone) epoxy. These constituents are shown in Fig. 3 and 4 below.

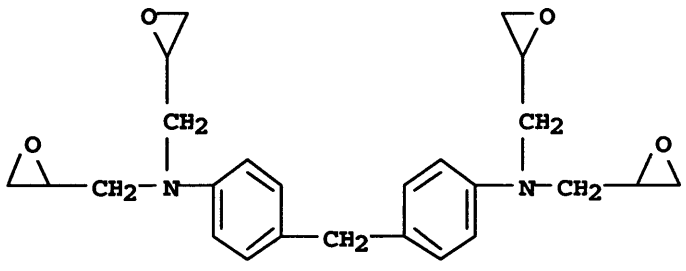

Figure 3. Chemical structure of TGMDA

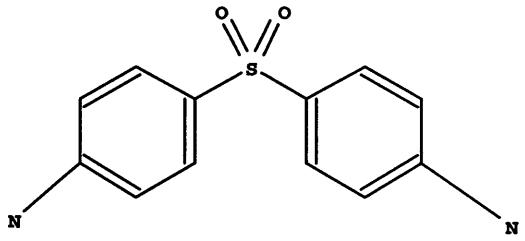

Figure 4. Chemical structure of DDS

This chemical structure is consistent with the FTIR (Fourier Transform Infrared Spectroscopy) scan which is described in next section.

3.2.2 FTIR Identification

FTIR is a technique that is widely employed for problems concerning the chemical composition of polymers. The FTIR experiment was conducted by Analytical Answers, Inc. The scan results are shown in the following Fig. 5. FTIR was also used to study the salient features of the resin curing reaction. Uncured, partially-cured and fully-cured samples were used to investigate the cure mechanism. For thermosetting polymer matrix composites, the prepreg must be stored in a freezer to prevent the matrix from curing at room temperature. The prepreg was stored in a freezer at $-30^{\circ}C$ until used. The functional groups related to the FTIR signal gave a close composition of TGMDA/DDS. The peak assignments in the FTIR are listed as follows:

1. 831.5: epoxy ring -C-C-O-;
2. 1614.4: -NH2;

3. Three peaks from 3242 to 3466: -NH2;

4. A broad peak at ~3400: -OH with hydrogen bonding;

5. Three peaks at ~3000: -CH-, -CH2-;

6. 1295.7: SO2.

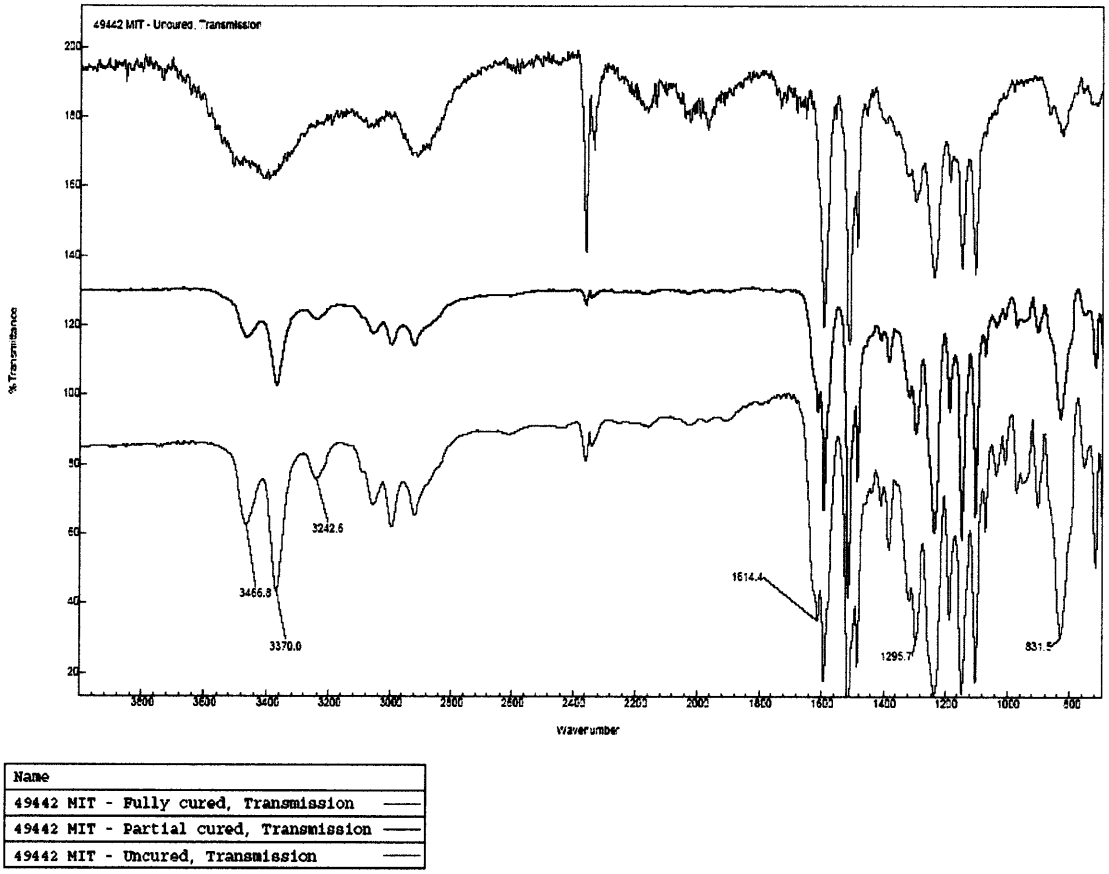

Figure 5. FTIR experimental results for the utilized epoxy resin

From the FTIR spectrum, we can see the peak of the epoxy ring -C-C-O- decreases with the curing process. We can also see that after the curing, the functional group -OH shows up. That is exactly because of the cure reaction between tetraglycidyl amine of methylene dianiline (TGMDA) and diaminodiphenyl sulfone (DDS). It is

assumed that all these three samples have the same thickness and concentration. The signal of -CH and -CH2 should not change if the curing temperature is not too high. But since it changes in the spectrum, most likely it will happen to the fully-cured sample. That is what we have seen. The partial and fully cured samples have similar signal intensity, but much smaller than the original one. It is due to the thickness loss and other factors during curing process.

From the Fourier Transform Infrared Spectroscopy (FTIR) scan results, we can observe those functional groups in TGMDA and DDS, and also the cure reaction between TGMDA and DDS. So it is reasonable to regard the prepreg formulation of this epoxy resin to be based on TGMDA and DDS.

3.2.3 DSC and TGA Analysis

Both Differential Scanning Calorimetry (DSC) and Thermogravimetric Analysis (TGA) were used for the analysis of high temperature behavior of the given resin. In order to observe the thermal transitions and discover what structural change was occurring within the polymer, DSC tests were performed using TA 800 DSC machine in the Processing and Characterization Laboratory at the Institute for Soldier Nanotechnologies (ISN). The sample is 5mg of CYCOM 977-3 prepreg. The temperature sweep began at $25^{\circ}C$ and ended at $300^{\circ}C$, and entailed a slow heating rate of $5^{\circ}C/\min$. The result is shown in Fig. 6 and depicts a gradual exotherm that begins at approximately $180^{\circ}C$. It is likely that this exotherm corresponds to a crosslinking event within the polymer. Thus, the glass transition temperature T_g can be considered approximately $180^{\circ}C$ from the DSC test. At approximately $270^{\circ}C$, a large endotherm was observed in the DSC scan.

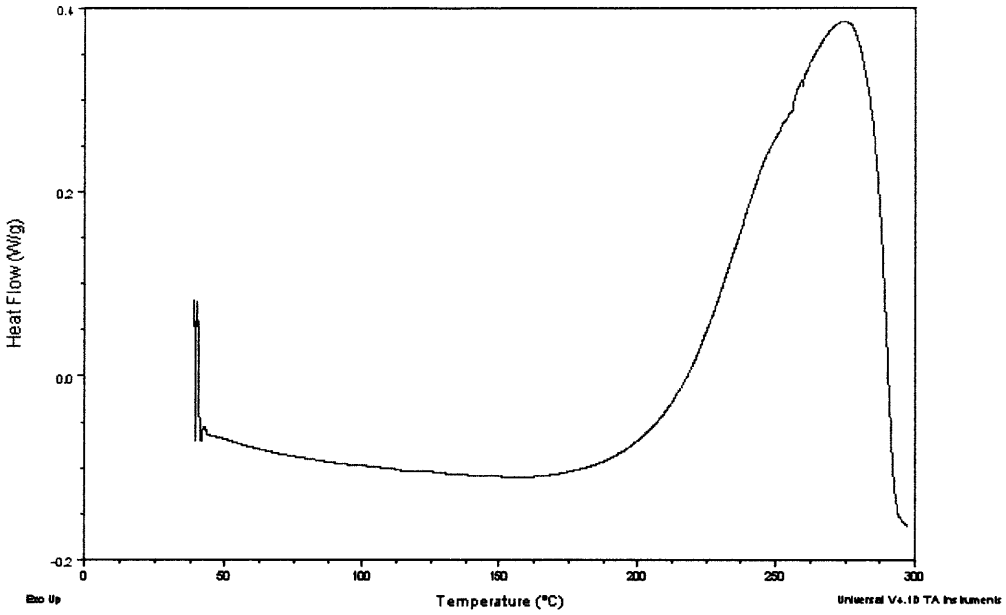

Figure 6. DSC experimental results for the utilized epoxy resin

In order to measure the weight change in materials as a function of time and temperature, TGA tests were performed using Perkin-Elmer TGA-7 Thermogravimetric Analyzer at the Center for Materials Science and Engineering at MIT. The temperature sweep began at $0^{\circ}C$ and ended at $500^{\circ}C$ in a nitrogen atmosphere. The ramping rate in the TGA experiments was $10^{\circ}C/\min$. The result is shown in Fig. 7. The resin began to lose weight at approximately $180^{\circ}C$ and has a transition at approximately $260^{\circ}C$, which coincides with the DSC results. A weight loss of twenty percents was observed at $500^{\circ}C$. So the fiber weight fraction is estimated at approximately eighty percents.

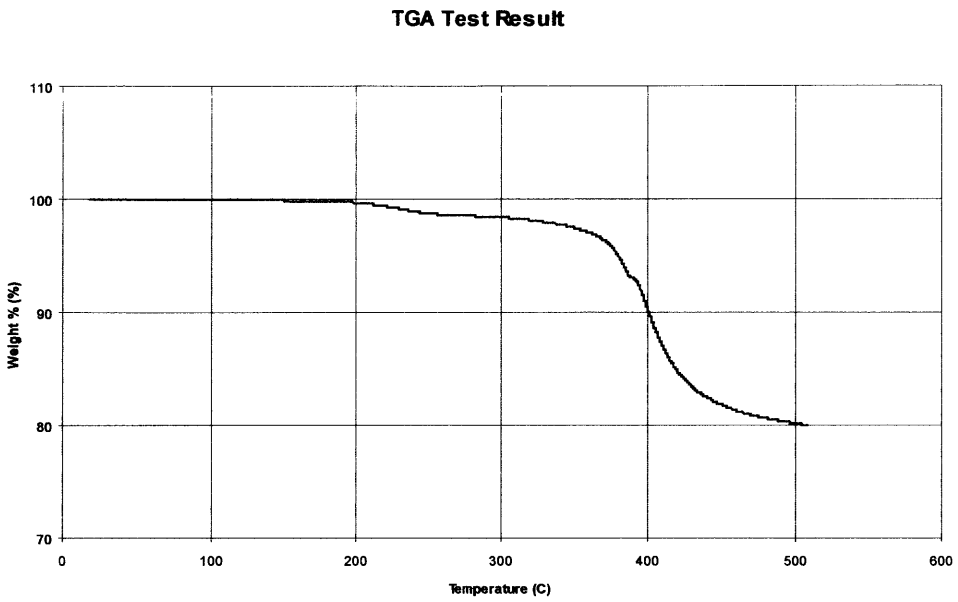

Figure 7. TGA experimental results for the utilized epoxy resin

3.2.4 DMA for Viscoelastic Response

Dynamic Mechanical Analysis (DMA) was conducted to study the dynamic mechanical properties. DMA tests were performed using TA 1000 DMA machine in the Processing and Characterization Laboratory at the Institute for Soldier Nanotechnologies (ISN). 8 plies were layered for the set-up of dynamic compression mode. The frequency was fixed at 1 Hz and the temperature was swept from $25^{\circ}C$ to $230^{\circ}C$. The result is shown in Fig. 8. The peak of the loss modulus shows us a glass transition occurring at approximately $50^{\circ}C$. However, glass transition has dependence on the frequency. We cannot simply compare this result with the DSC result.

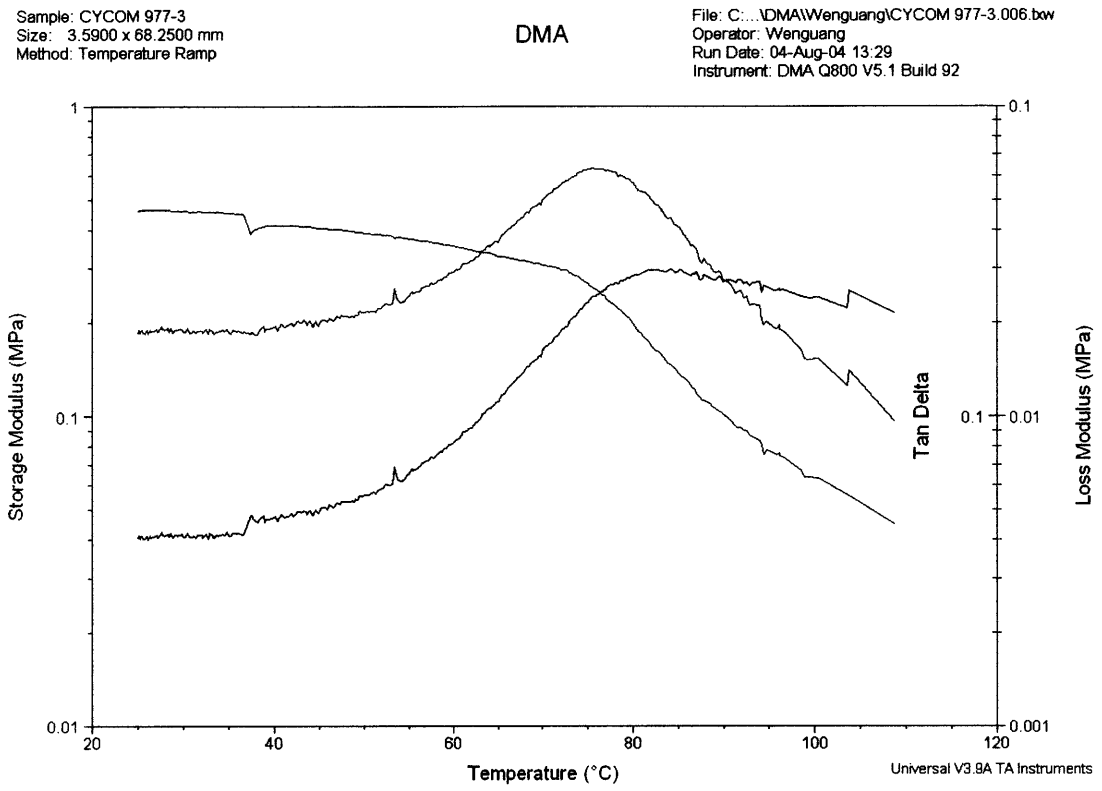

Figure 8. DMA experimental results for the utilized epoxy resin

Roylance et al. developed an analytical model, which provides a means of extrapolating the viscoelastic dissipation from the low frequencies of the DMA characterization to the higher ultrasonic frequencies in actual processing. The prepreg utilized in the previous study was impregnated with Hexcel Corporation's 8552 thermoplastic-toughened high-performance epoxy resin. From our DMA tests, the viscoelastic properties of Cytec 977-3 are shown close to those of 8552 resin. So the viscoelastic parameters obtained in the previous study were used for this UTL simulation.

From the early work done by Roylance [9], the Wiechert model fit for the carbon/8552 composite gave the numerical values of τ_{0j} and k_j as follows:

τ_{0j}	k_j
8.87E-11	1.11E+06
8.87E-12	5.56E+06
8.87E-13	1.03E+07
8.87E-14	2.50E+07
8.87E-15	8.42E+07
8.87E-16	2.10E+08
8.87E-17	2.87E+07

The activation energy was determined by the line slope of the Arrhenius plot for the DMA date to be E^{τ} =69.1 kJ/mol. The loss modulus can be computed at any given temperature and frequency, which provide us a good tool to extrapolate the viscoelastic response of the low frequencies from DMA to the high frequencies under ultrasonic loading.

Chapter 4

Finite Element Analysis Results

4.1 Finite Element Model

The model used to simulate the UTL process is shown in Fig. 9. The computational sample consists of two layers of 360 microns thick, CYCOM 977-3, carbon fiber epoxy prepreg. The orientation of the first layer is [0] and that of the second layer is [+45/-45].

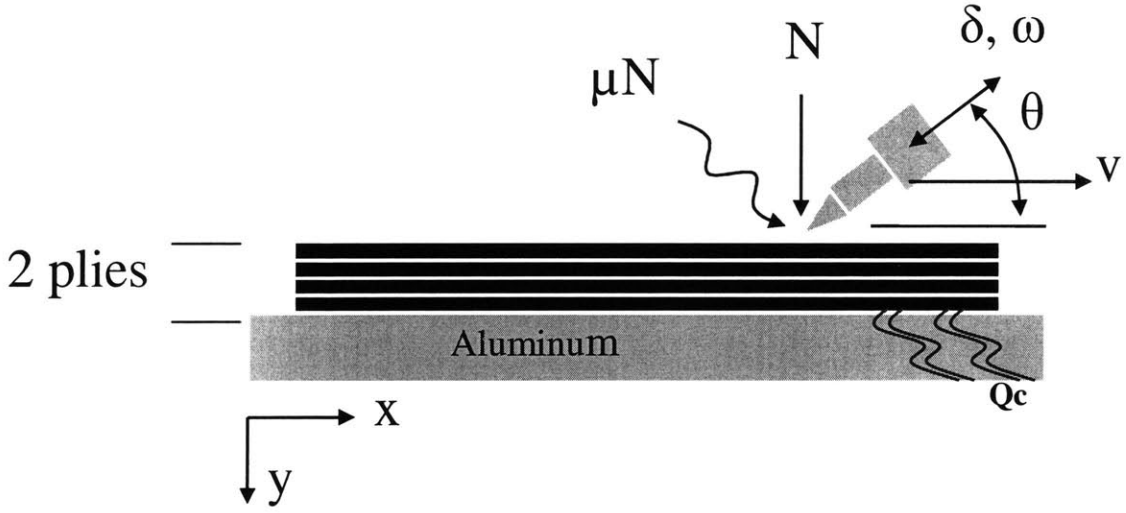

Figure 9. Cross-section of the 2-layer carbon epoxy laminates

The frequency of the ultrasonic horn is 30 KHz. The amplitude is 16 microns and the contact load is 6.4 lbs. The horn angle θ is 30°. These are chosen to match the experimental setup provided by Foster-Miller Inc. The density is chosen as 2000 kg/m^3 and the specific heat is chosen as 116 $J/kg-^{\circ}C$ for the given resin.

In heat transfer analysis, it is necessary to provide thermal conductivity of the material. We considered a transversely isotropic case for our composite model, so we only need provide K_{xz} and K_y. For the first layer of [0] orientation, K_{xz} is set as 18.0 $W/m-^{\circ}C$ and K_y is set as 0.95 $W/m-^{\circ}C$. For the second layer of [+45/-45] orientation, K_y doesn't change and K_{xz} changes to 9.475 $W/m-^{\circ}C$. This is because of the change of the fiber orientation on the x-z plane.

The manufacturer-supplied material properties of this kind of composite laminates are given in Table 1:

Mechanical Properties	-60°F	RT	104°F		121°F		132°F		149°F	
			Dry	Wet	Dry	Wet	Dry	Wet	Dry	Wet
0° Tensile Properties										
Strength, MPa	2430	2510								
Modulus, GPa	158	162								
Strain, %	1.52	1.46								
90° Tensile Properties										
Strength, MPa		64.1								
Modulus, GPa		8.34								
Strain, %		0.77								
0° Compressive Properties										
Strength, MPa		1580		1520[1]		1340[1]		1240[1]		1100[1]
Modulus, GPa		154	147	146[1]	141	146[1]	139	156[1]	148	150[1]
Open Hole Compression										
Strength, MPa		322		225[2]		241[2]				
(25/50/25 orientation)										
0° Interlaminar Shear Properties										
Strength, MPa		127	93.6	88.9[1]	91.7	78.6[1]	85.5	69.6[1]	78.6	62[1]
In-Plane Shear Properties										
Modulus, MPa (+45)		4.96		4.21[3]		4.00[3]		3.45[3]		2.34[3]
Weight Gain = 0.9%										
0° Flexural Properties										
Strength, MPa		1765	1700	1200[1]	1524	1120[1]	1500	965[1]	1420	862[1]
Modulus, GPa		150	153	139[1]	143	146[1]	145	135	145	130
90° Flexural Properties										
Strength, MPa		131								
Modulus, GPa		8.20								
Edge Delamination Strength, MPa										
Onset		255								
Ultimate		634								
Compression After Impact, MPa										
(25/50/25 orientation		193								
270 in-lb impact level)										
Interlaminar Fracture Toughness										
G_c (DCB), in-lb/in		1.8								
G_c (ENF), in-lb/in		3.3								

Table 1. Typical properties of the used composite laminates

For the first layer of [0] orientation, elastic modulus is 162 GPa, the shear modulus is 4.96 GPa, and the Poisson's ratio is 0.27; for the second layer of [+45/-45] orientation, the elastic modulus is 16.94 GPa, the shear modulus is 41.6 GPa, and the Poisson's ratio is 0.806. Both the thermal conductivity and material constants of the second layer are calculated from the composite theory.

4.2 Geometry and Boundary Conditions

In order to investigate the effect of mesh density on the results, the models are created using different number of 4-noded quadrilateral elements. Due to the large number of calculations required, a relatively coarse 10x10 mesh of 100 elements is used as a first approximation. The geometrical size is 600 microns wide and 360 microns thick. This mesh allows the whole process to be simulated at a lower computational cost. It is also easier to compare with the analytical results for only the displacements and stresses using this kind of regular mesh.

Considering the concentrated load of the ultrasonic horn, a finer 20x15 mesh of 300 elements with density gradient is created. The geometrical size is 800 microns wide and 360 microns thick. The mesh is shown in Fig. 10. Little variations with respect to mesh density are observed.

In the finite element simulation, the bottom boundary of the model is fixed for both displacements and temperature. The temperature is set as room temperature at $23\,^{\circ}C$. The displacements on both sides are fixed and the temperature is set as free. It is important to examine the boundary effect of on the heat transfer to prepreg lay-up. Bogetti and Gillespie studied the effect on glass-polyester curing process. In their

research, convention boundary conditions were considered using the same finite element mesh [10]. They stated that the rate of heat loss from the surface by convection to the air is slow enough so that one can neglect it. In our finite simulation, we neglected the convection from the surface.

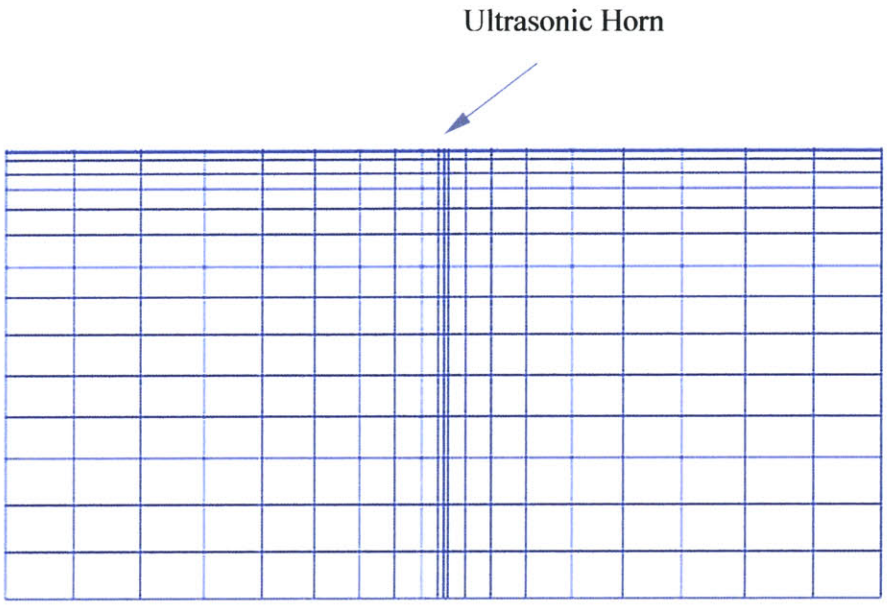

Figure 10. Two-dimensional finite element model in gradient mesh

4.3 Time-Stepping Algorithm

The solution of time dependent problems requires the specification of a time increment, Δt. Two algorithms were used to control the size of the time increment during transient solutions. A logarithm time stepping followed by a regular time stepping is selected to achieve the desired accuracy. The logarithm time stepping helps us to catch the early viscoelastic response at a very small time interval at the beginning. It was found that the

finite element code we used is sensitive to the size of the time increment employed. To get a stable simulation result, sometimes we will have to combine the regular and the logarithm time stepping algorithms.

4.4 Simulation Results

Results of numerical simulation are shown in this section using a more functional and powerful post-processor. It was developed for the FEA code to plot the 2-D images of the transient displacements, temperature, and strains at different time steps. It can also plot the strain energy, dissipation, and deformed mesh.

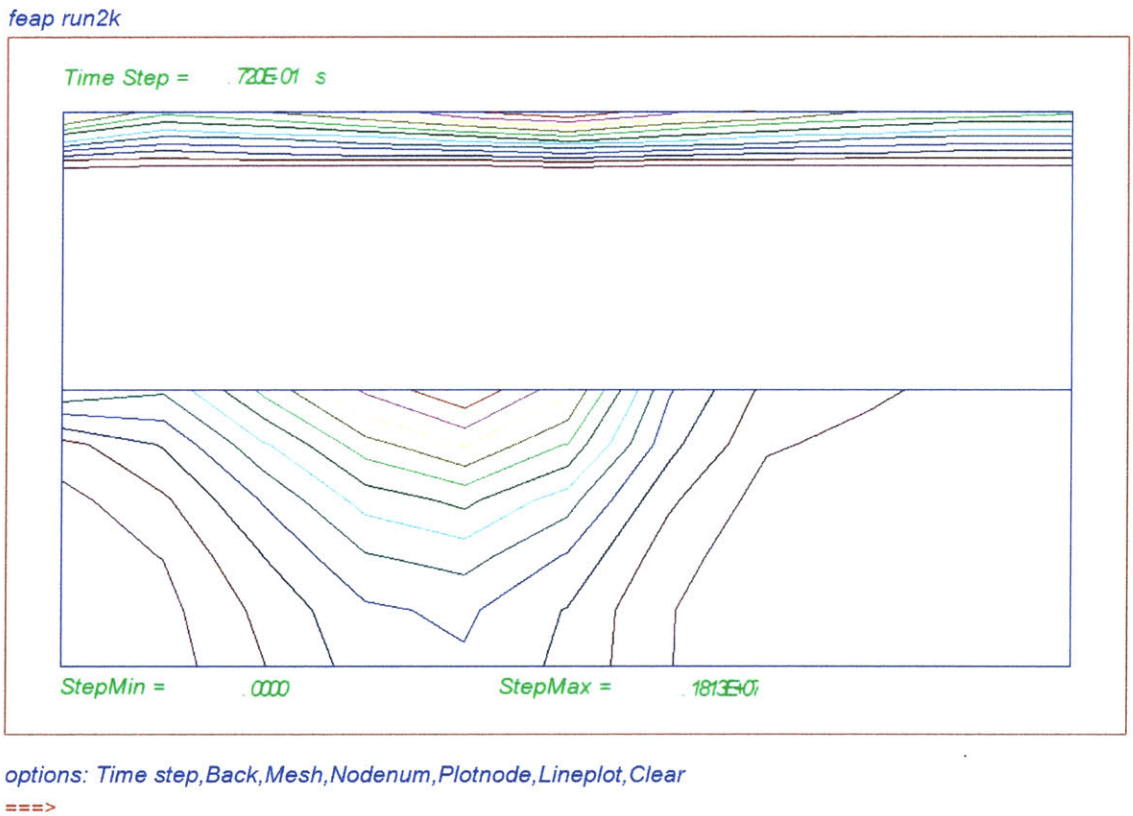

Figure 11. Plot of heat generation rate Q for the UTL simulation

Viscoelastic dissipation to the prepreg is plotted in Fig. 11. Since composites are anisotropic, heat is conducted along the fiber faster than transverse to them. The dissipation contours predicted by the finite element program are therefore, elongated in the fiber direction for the first layer with the orientation of [0]. For the second layer with the orientation of [+45/-45], the dissipation distributed much more in the thickness direction. Because there is convection from the surface, we got some very small negative dissipation in our simulations. However, such convection is so small that we can neglect them.

The temperature contours in the laminates obtained from the finite element analysis are illustrated in following Fig. 12 and 13:

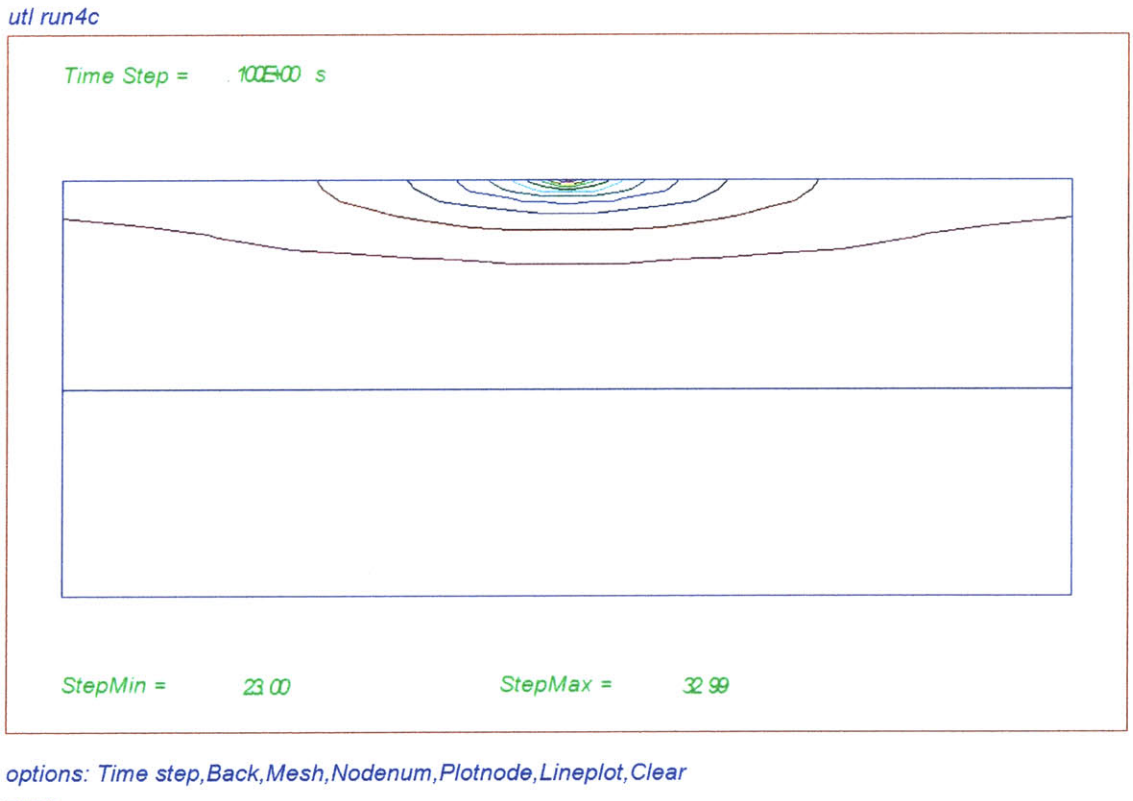

Figure 12. Contour plot of temperature field at t=0.1s

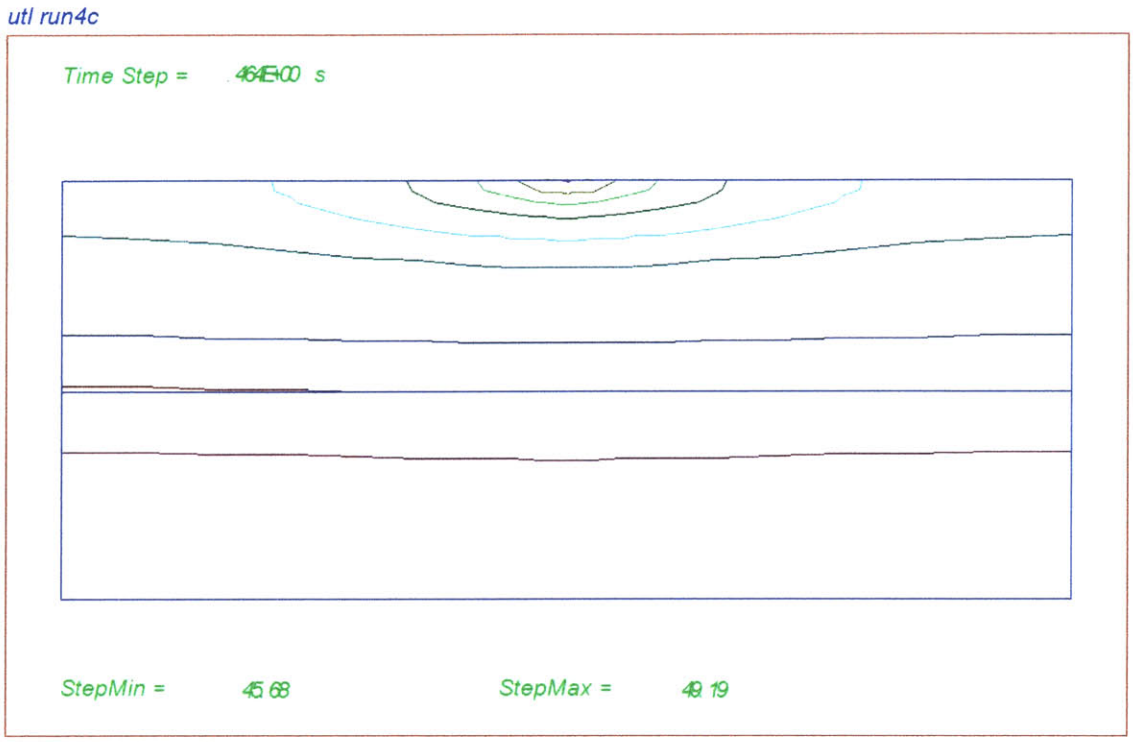

Figure 13. Contour plot of temperature field at t=0.464s

Due to the heat transfer from the tip to the bottom composite, temperatures at the ultrasonic loading point were higher than those at other positions. Temperature contours are also elongated in the fiber direction.

Because the preload is displacements of 16 microns at the horn angle of $30^{\circ}C$, the strain response is slightly different for different size of computational specimen. Hence the strain energy and the viscoelastic dissipation change. We increase the size 100 times larger and run the simulation again to see the change of the penetration depth for the dissipated strain energy level, the temperature contours are shown in following Fig. 14 and 15:

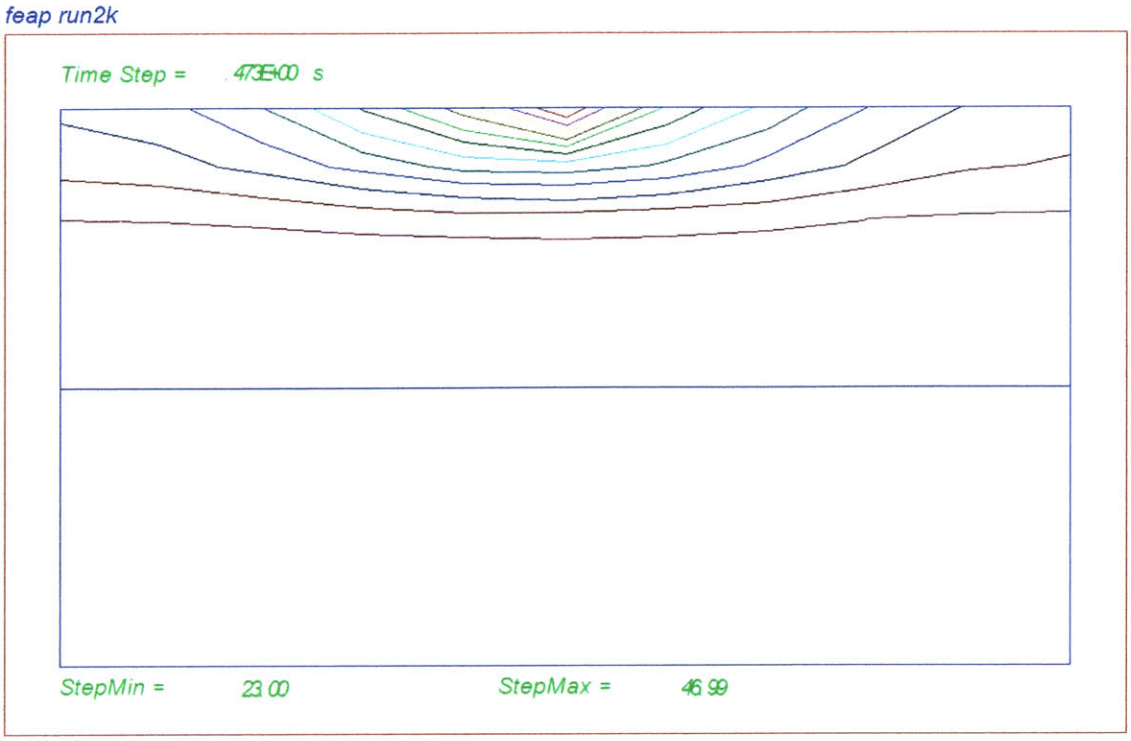

Figure 14. Contour plot of temperature field at t=0.473s for large geometry

In Fig. 13, the maximum temperature of the small size computational specimen is $49.19^{\circ}C$ and the minimum temperature is $45.68^{\circ}C$ at 0.464 seconds. In Fig. 15, the maximum temperature of the large size computational specimen is $46.99^{\circ}C$ and the minimum temperature is $23^{\circ}C$ at 0.473 seconds. The change of the plots is mainly because the penetration depth at the given energy level becomes small comparing with the large geometrical size. As we stated before, for different UTL specimen, to provide the balanced energy input, the amplitude and horn angle should be optimized.

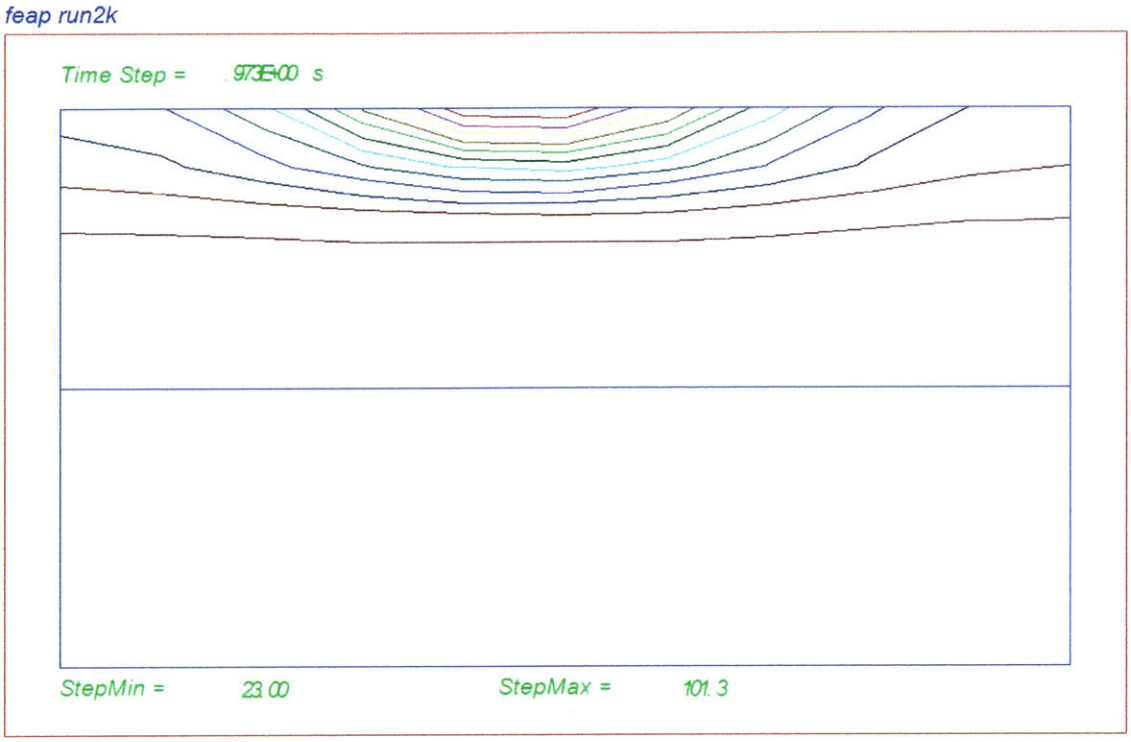

Figure 15. Contour plot of temperature field at t=0.973s for large geometry

At about 1 second, the maximum temperature was $101^{\circ}C$. Because the curing temperature of CYCOM 977-3 is about $177^{\circ}C$ and the temperature fields in the UTL simulations are below the curing temperature, this permits the laminate to be consolidated prior to full curing in an autoclave or other equipment.

Fig. 16 presents the variation of temperature with time. In next section the experimental results of an experimental validation test with 10 seconds welding time are compared to the numerical predictions for the same parameters. However, in their experimental setup, they are moving the horn at the speed of 1m/s so that the composite won't be burned off by the high local temperature. In the UTL simulation, we turned off

the ultrasonic horn after 1 second and set the temperature back to the room temperature at $23^{\circ}C$. Otherwise the temperature will be too high and damage the composite. The peak temperature we picked up is enough for us to compare with the experimental data.

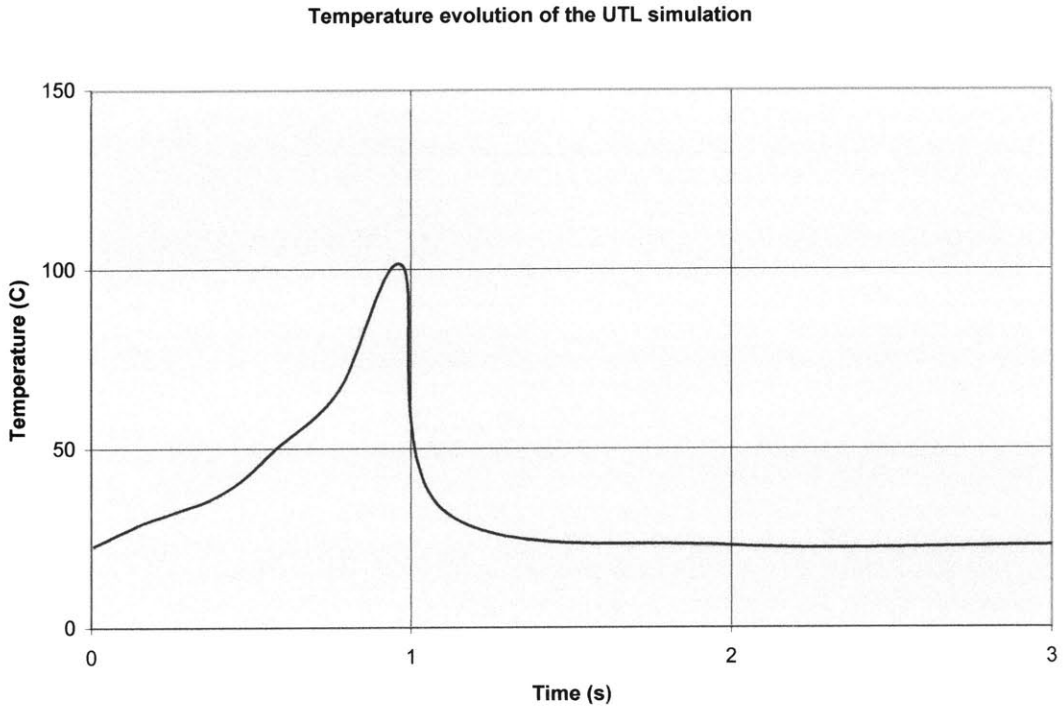

Fig. 16 The variation of temperature with time of UTL simulation

4.5 Experimental Validation

Foster-Miller Inc. performed a static experiment to measure the temperature field of CYCOM 977-3 prepreg during ultrasonic processing. The results of the experiment are compared to that of the finite element simulation for the same parameters. The frequency

of the ultrasonic horn is 30 KHz. The amplitude is 16 microns and the contact load is 6.4 lbs. The horn angle θ is 30°.

The experimental setup of the static validation test is shown in Fig.17.

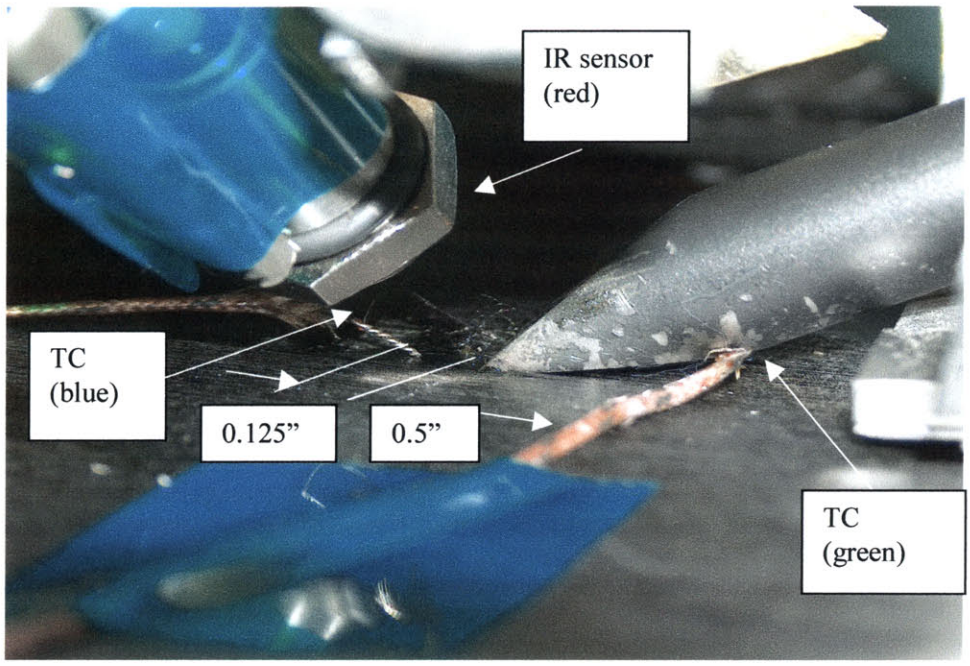

Figure 17. Photo of the static validation test

The temperature is measured by an infrared (IR) sensor in front of the horn and two surface contact thermocouples (TC) in front of and behind the ultrasonic horn.

The surface temperature data from the static experiment is shown in Fig. 18. The weld time for the static experiment is about 10 seconds. That is why the temperature dropped around 11 seconds and back to the room temperature.

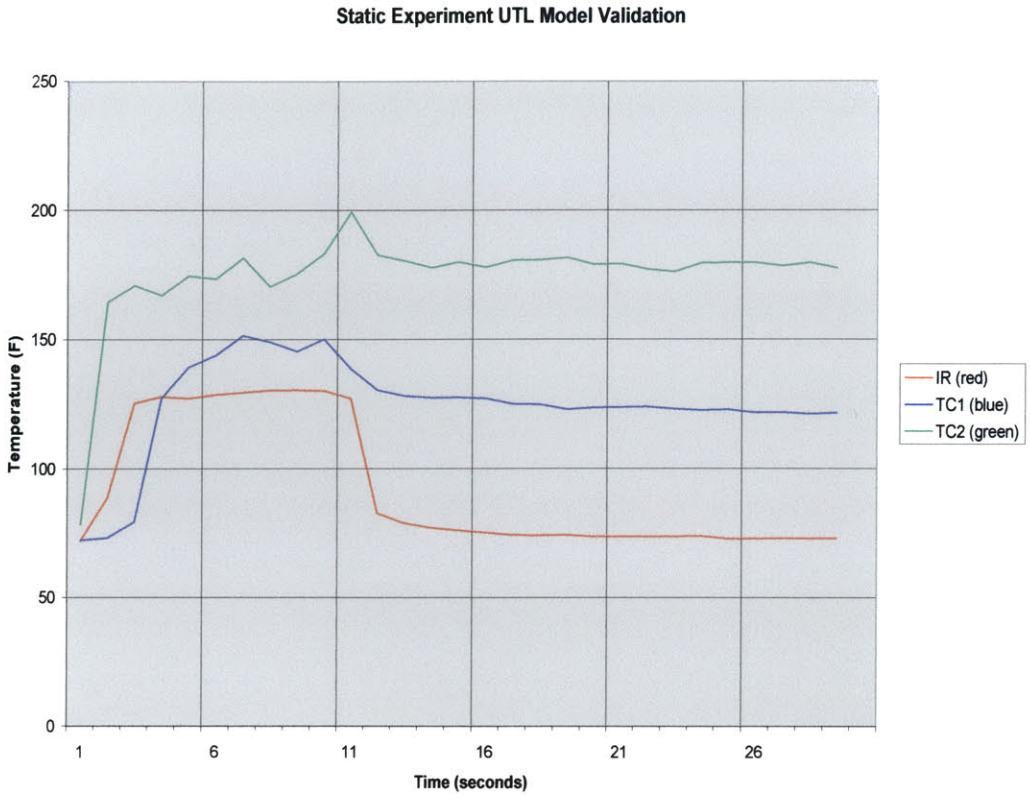

Figure 18. Temperature data from static UTL experiment

A comparison of the experimental and computational is shown in Fig. 19. It is obvious that the prediction introduced a very fast dissipation comparing with all of the experimental data. Given the slow climb of the experimental data, this may because of the over-simplification of the numerical model and/or the limit of the sensor to catch the start-up temperature of the UTL process. There are refinements that would likely reduce the error between the prediction and the observed temperatures. However, it would be interesting to see if the temperature field within a second is closer to prediction. Unfortunately, most available experimental methods cannot catch the temperature profile in such a short time period. Advanced sensing system is needed for further research. More detailed discussions and recommendations will be presented in Chapter 5.

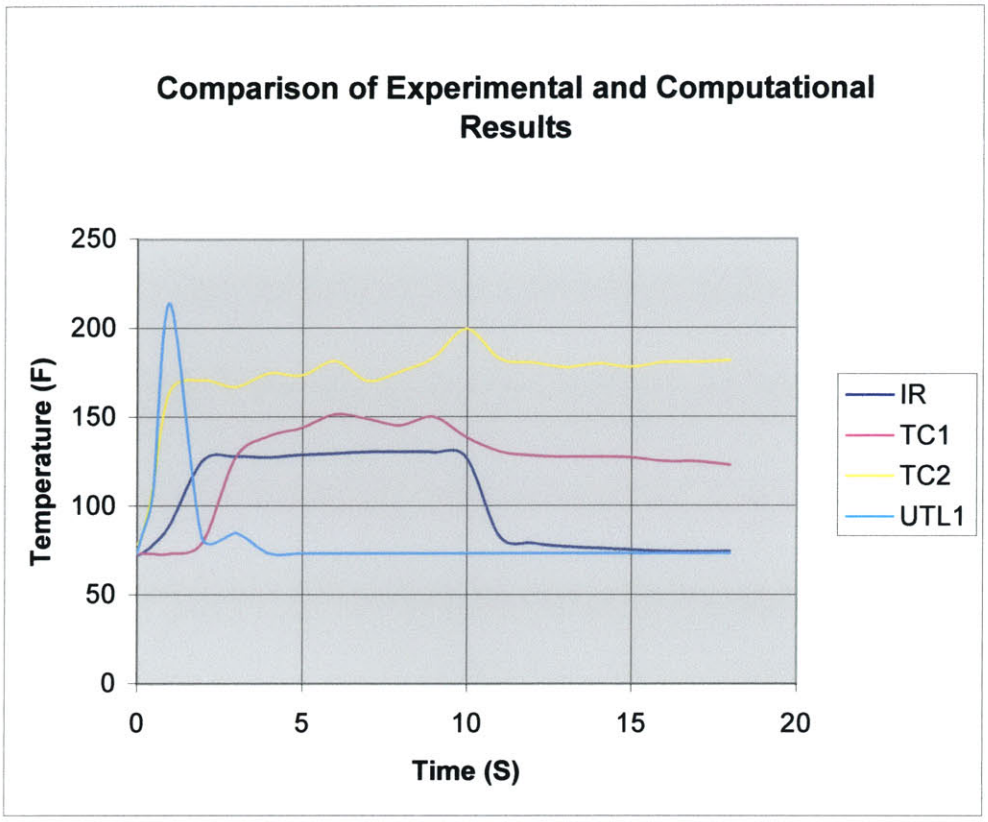

Figure 19. Comparison of experimental and computational UTL results

4.6 Analytical Validation

To validate the displacement fields of the UTL simulation, we compared the simulation results with Flamant solution for 2D case with point force normal to semi-infinite elastic space.

The analytical expression of Flamant solution is listed below:

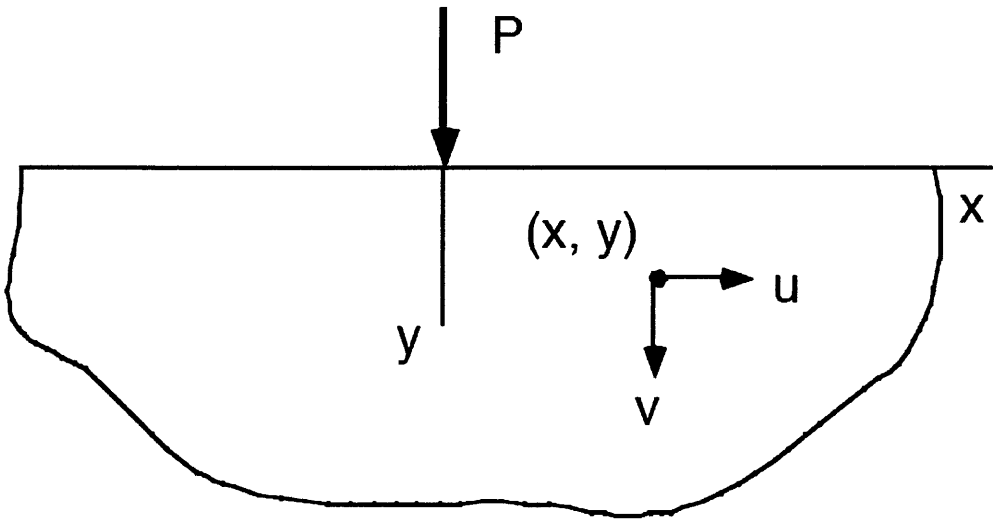

Figure 20. Flamant Solution for 2D case

$$u = -\frac{P}{4\pi\mu}\left\{(\kappa-1)\theta - \frac{2xy}{r^2}\right\}, \quad v = -\frac{P}{4\pi\mu}\left\{(\kappa+1)\log r - \frac{2y^2}{r^2}\right\}$$

μ : elastic shear modulus, ν : Poisson's ratio

κ : Dundars constant

$= 3-4\nu$, for plane strain; $= (3-\nu)/(1+\nu)$, for plane stress

$r = \sqrt{x^2+y^2}$, $\tan\theta = x/y$

The displacements from Flamant solution are plotted in Fig. 21 and 22.

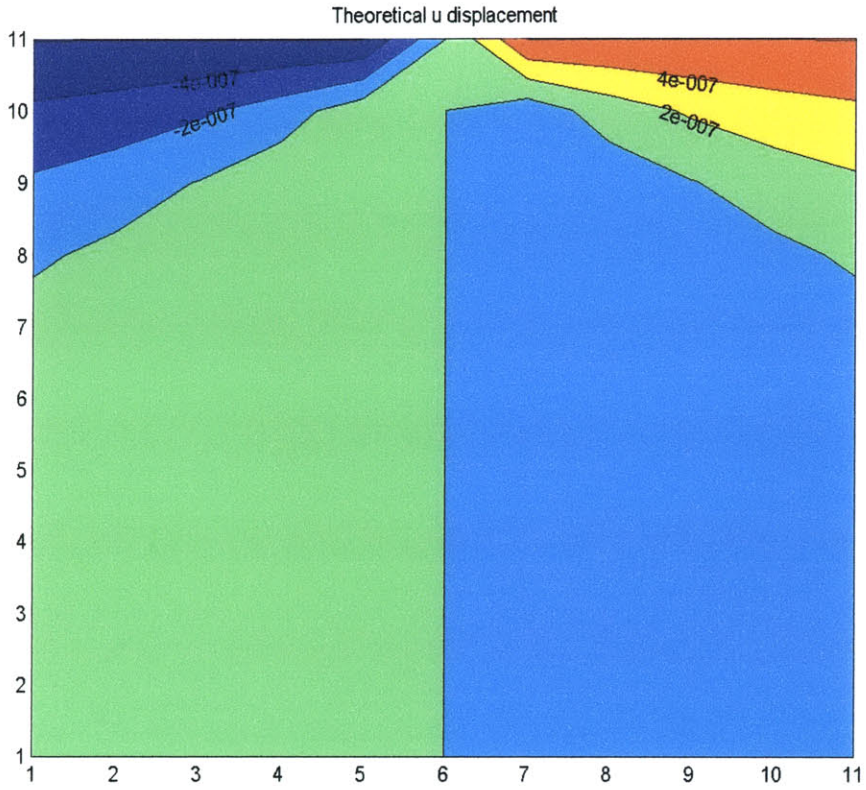

Figure 21. Plot of u displacement from Flamant Solution for 2D case

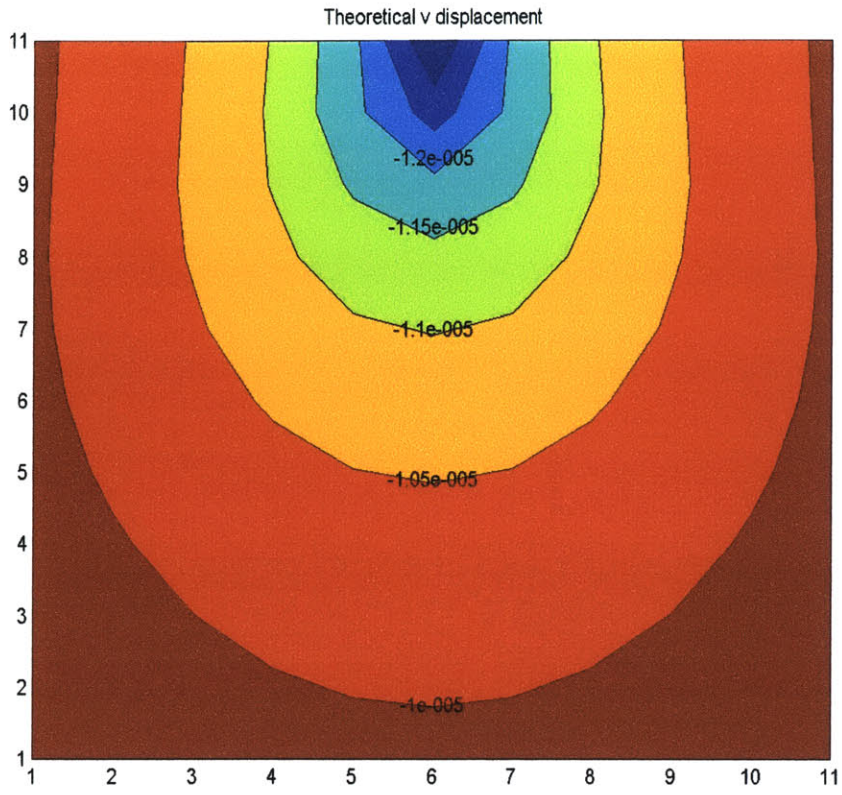

Figure 22. Plot of v displacement from Flamant Solution for 2D case

The excitation source of numerical simulation is changed to a unit force at the normal direction instead of horn angle of 30° only for validation purpose. The displacements from UTL simulation are plotted in Fig. 23 and 24.

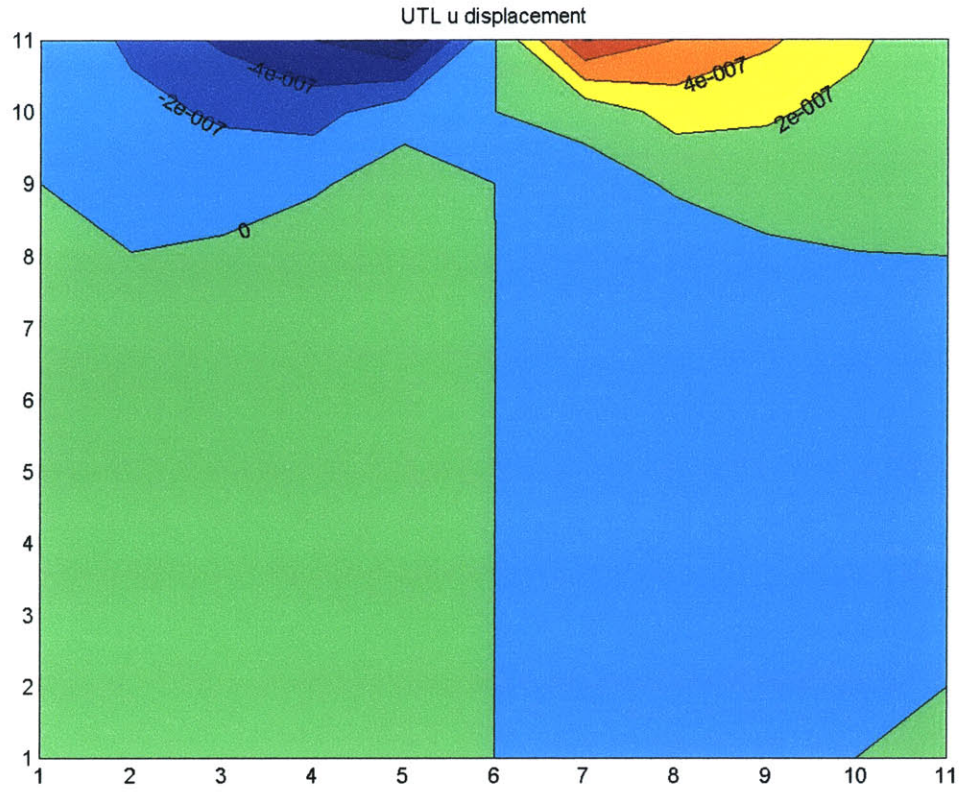

Figure 23. Plot of u displacement from UTL simulation

From the plots, we can see a close match between the Flamant solution and UTL simulation for unit normal load.

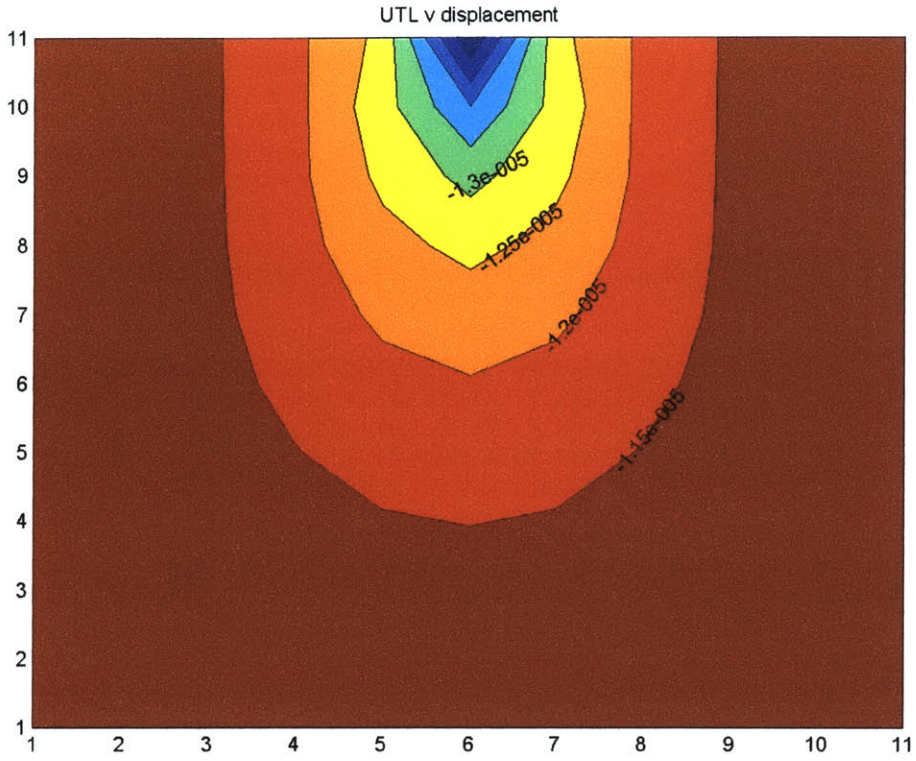

Figure 24. Plot of v displacement from UTL simulation

In order to further validate the computation of the displacement fields from UTL, we used Flamant solution to compute the vertical displacements of those nodal points along the line of the horn loading point for the 10x10 regular mesh and compared the results with the UTL simulation with all the same parameters. The comparison is shown in Fig. 25. The computational results gave an acceptable match to the theoretical solution.

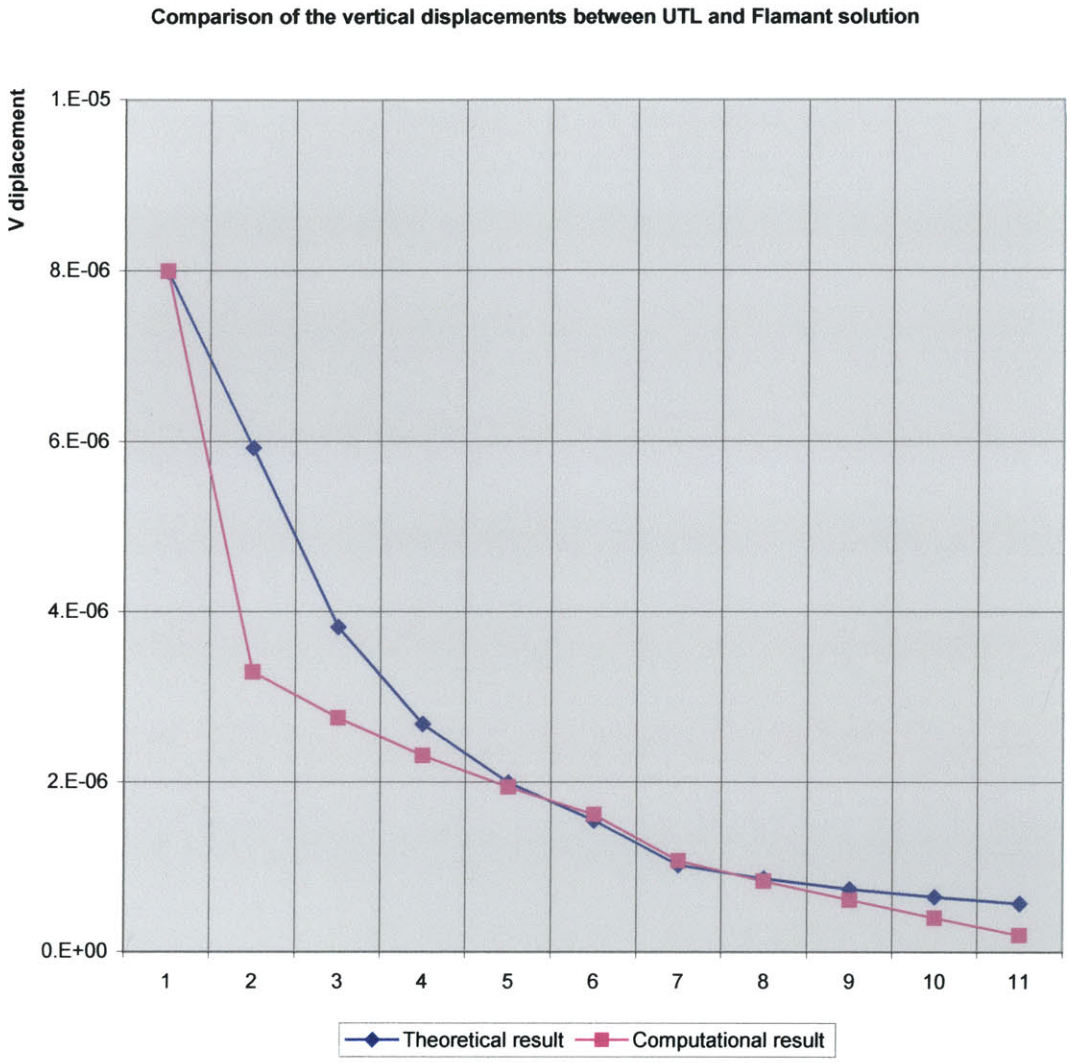

Figure 25. Comparison of the vertical displacements between UTL and Flamant solution

Chapter 5

Conclusions and Recommendations

Transient heat transfer finite element code is developed to simulate the ultrasonic processing of polymer matrix composites. It can handle the UTL simulation incorporating a number of the experimental variables – horn angle, oscillation amplitude, velocity of horn along the surface, thickness and material properties of the laminate, etc. Although we are currently using the model to predict temperature fields based on a static ultrasonic horn, the model is capable of calculating the transient temperature distribution for dynamic horn motion. Please refer to appendix A to see the plot of UTL simulation with moving horn for one layer model.

The comparison between experimental and simulation results showed that the predicted temperature profiles was ahead of the experimental data provided by Foster-Miller Inc. The discussion is presented below:

From the experimental point of view, Foster-Miller Inc. stated that the data acquisition limit of their current IR sensor system (~250 milliseconds) makes it difficult to sufficiently characterize the start up transient temperatures of the UTL process. Foster-Miller has pursued the implementation of a higher response rate control system so that high rates of UTL compaction can be accomplished in line with the fiber placement process. Once the high response rate control system is installed, it may be possible to have sufficient data acquisition rates to validate the model's start up transient predictions.

Numerical results show that the transient temperature is sensitive to small changes in time step size. Boundary condition also significantly influences the temperature distribution. So there will be errors based on these factors.

The model neglected the effects of convection from the surface to the air. The convection component is potentially more significant depending on the air flow. Radiation is also not considered to be significant at the temperatures we are processing the thermoset materials.

Another factor that is not included in the model currently is the static pressure applied through the horn. This means that friction as a source of heat generated is also not included. We supposed that viscoelastic heating dominates the UTL heat generation in the polymer prepreg and the contact pressure has no obvious effect.

These factors will be added as the model is being refined. Given the slow climb of the experimental, it is likely the addition of the convection to the air would decrease the heat dissipation at the surface. This would likely help the prediction to cool off and match the experimental results better.

References

1. A. Johnston et al. "Finite Element Analysis of Autoclave Processing of Large Composite Structures Using a Substructuring Technique," Proceedings of the 28th International SAMPE Technical Conference, pp. 734-744. (1996)
2. H. Pascal et al. "A Two-Dimensional Flow Model for the Process Simulation of Complex Shape Composite Laminates," International Journal for Numerical Methods in Engineering, Vol. 44, pp. 1-26. (1999)
3. M. E. Roylance, D. K. Roylance and K. L. Nesmith, "Use of Ultrasonic Tape Lamination for In-Process Debulking of Thick Composite Structures," Proceedings of the 43rd International SAMPE Symposium and Exhibition. (1998)
4. M. N. Tolunay, P. R. Dawson and K. K. Wang, "Heating and Bonding Mechanism in Ultrasonic Welding of Thermoplastics," *Polymer Engineering and Science*, Vol. 23, No. 13, pp. 726-733. (1981)
5. S. Y. Pusatcioglu, J. C. Hassler, A. L. Frickle and H. A. MeGee Jr., "Effect of Temperature Gradients on Cure and Stress Gradients in Thick Thermoset Castings," *Journal Applied Polymer Science*, Vol. 25, pp. 381-393. (1980)
6. W. I. Lee, A. C. Loos and G. S. Springer, "Heat of Region, Degree of Cure, and Viscosity of Hercules 3501-6 Resin," *Journal of Composite Materials*, Vol. 16, 510-520. (1982)
7. L. Aylward, C. Douglas, and D. Roylance, "A Transient Finite Element Model for Pultrusion Processing," *Polymer Process Engineering,* vol. 3, pp. 247-261. (1985)

8. Roylance, D., L. Chiao, and P. McElroy, "Versatile Finite Element Code for Polymer Composite Processing," *Computer Applications in Applied Polymer Science, II: Automation, Modeling, and Simulation*, ACS Symposium Series, No. 404, pp. 270 – 280. (1989)

9. Roylance, M., J. Player, W. Zukas, and D. Roylance, "Modeling of Ultrasonic Processing," *Journal of Applied Polymer Science,* Vol. 93, pp. 1609-1615. (2004)

10. T. A. Bogetti and J. W. Gillespie Jr., "Two-Dimensional Cure Simulation of Thick Thermosetting Composites," *Journal of Composite Materials*, Vol. 25, 239-273. (1991)

11. W. B. Young, "Thermal Behavior of the Resin and Mold in the Process of Resin Transfer Molding," *Journal of Reinforced Plastic Composites*, Vol. 14, 310-332. (1995)

12. A. C. Loos and G. S. Springer, "Curing of Epoxy Matrix Composites" *Journal of Composite Materials*, Vol. 17, pp. 135-169. (1983)

13. A. C. Loos and J. D. MacRae, " A Process Simulation Model for the Manufacturing of a Blade-Stiffnened Panel by the Resin Film Infusion Process," *Composite Science and Technology*, Vol. 56, 273-289. (1996)

14. S. Yi et al. "A Finite Element Approach for Cure Simulation of Thermosetting Matrix Composites," *Computers and Structures*, Vol. 64. No. 1-4. pp. 383-388. (1997)

15. S. C. Joshi et al. "A Numerical Approach to the Modeling of Polymer Curing in Fiber-Reinforced Composites," *Composite Science and Technology*, Vol. 59, pp. 1003-1013. (1999)

16. O. C. Zienkiewicz, "The Finite Element Method," McGraw-Hill. (1997)

17. J. D. Ferry, "Viscoelastic Properties of Polymers," 3rd ed. Wiley & Sons, New York. (1980)

Appendix A UTL Output Plots

The post-processor was developed for the FEA code to plot the 2-D images of the transient displacements, temperature, and strains at different time steps. It can also plot the strain energy, dissipation, and deformed mesh at different time steps.

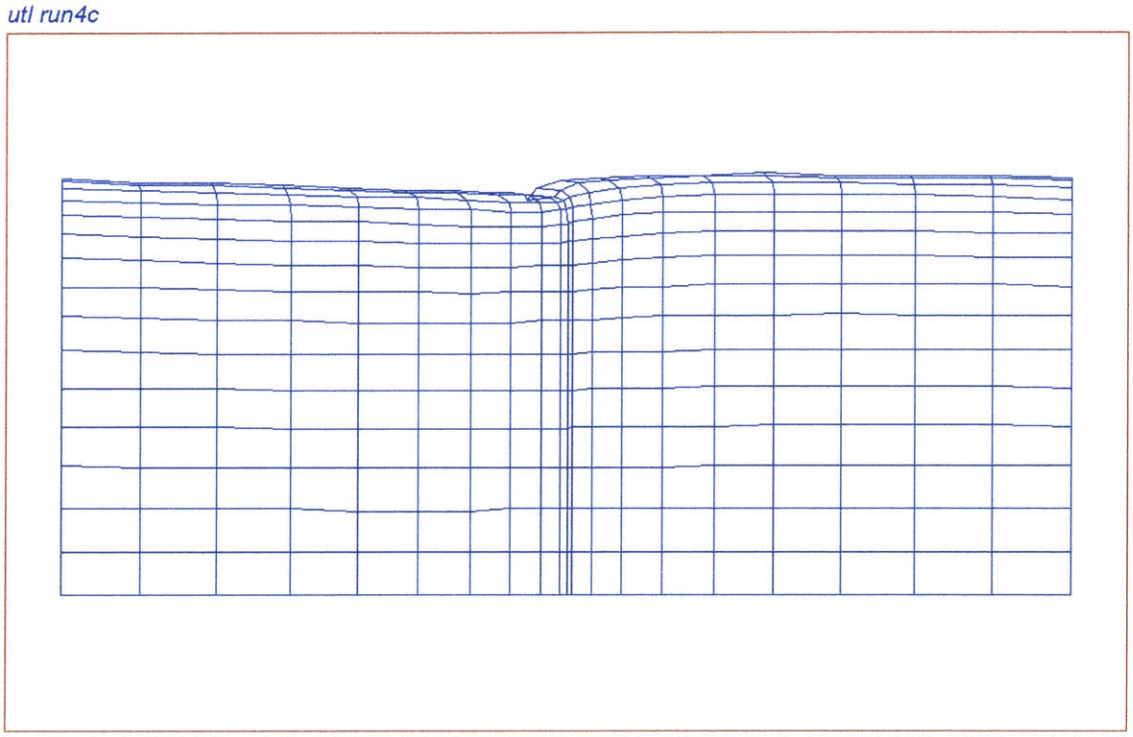

Fig. 26 The deformed mesh for UTL simulation

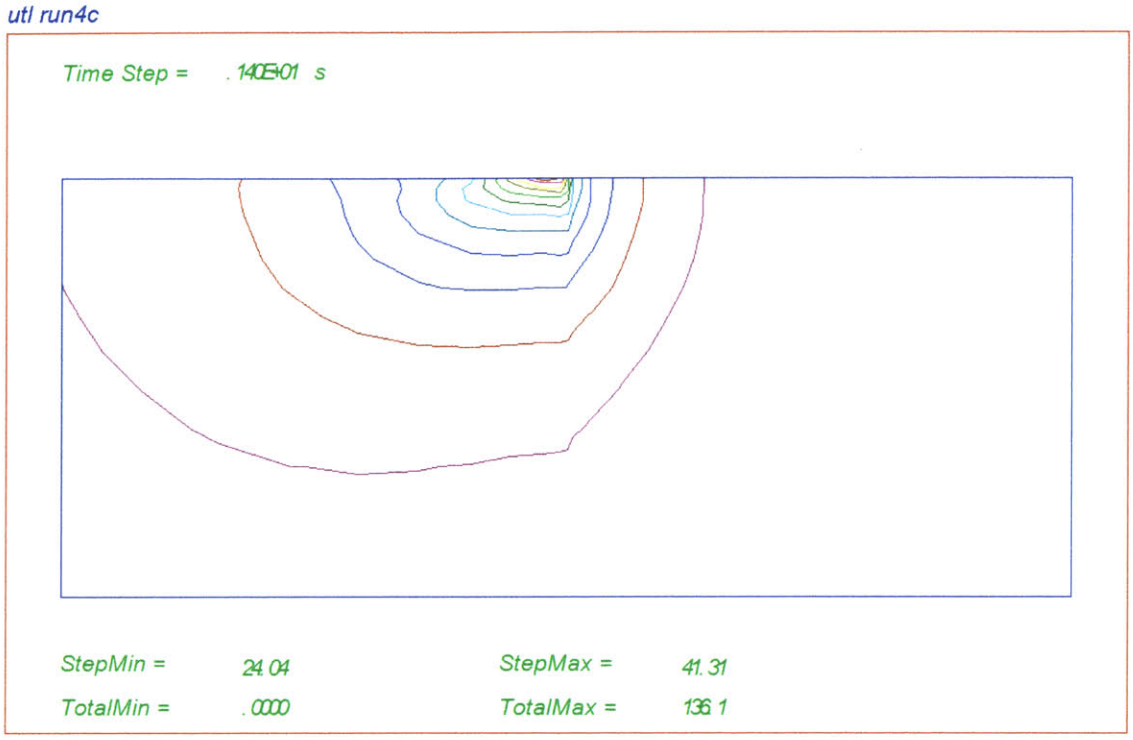

Fig. 27 The UTL simulation result with dynamic horn motion at t=1.4s for one layer model

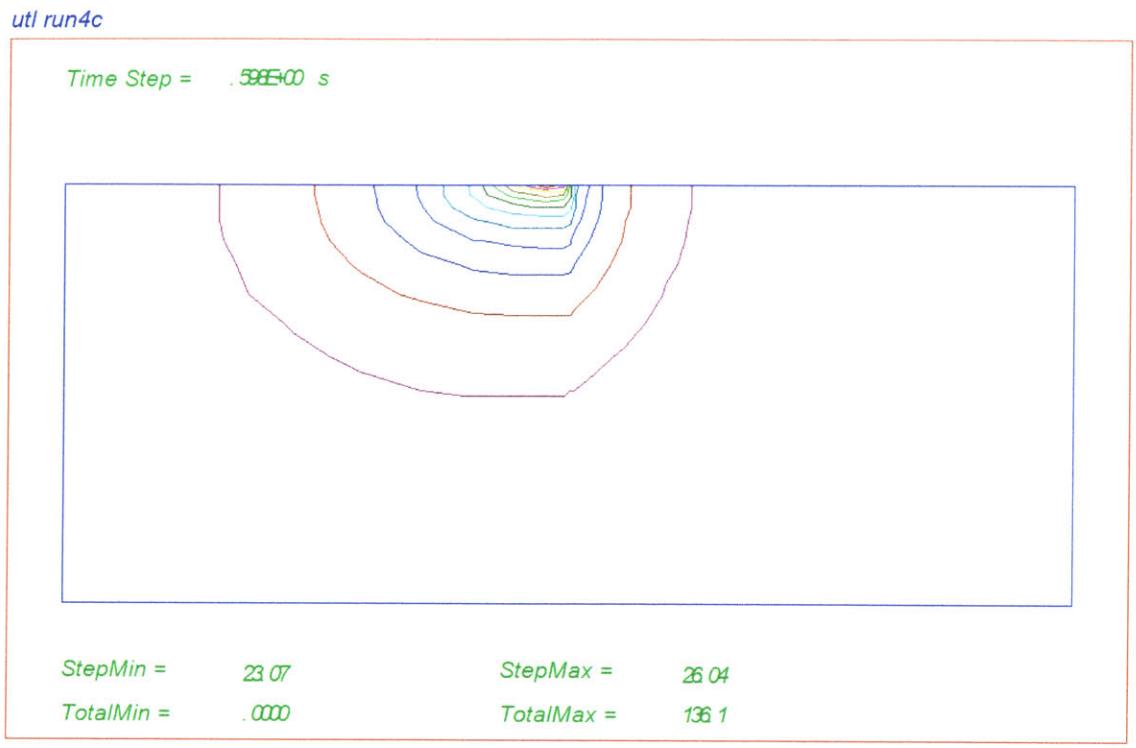

Fig. 28 The UTL simulation result with dynamic horn motion at t=6s for one layer model

Appendix B UTL Input File

The file listed below is the input file for the finite element package. It set up the geometry, material properties, boundary and loading condition, and the macro commands to solve the equations. The attached file is for the 20x15 mesh wish 300 four-noded elements. Please refer to Chapter 4 for more details about the finite element model.

```
feap run2k 10x10 mesh, d&T, ltim
  121  100    2    2    3    4    0
coor
    1    1-3.000E-04 0.000E+00
   11    0 3.000E-04 0.000E+00
   12    1-3.000E-04-3.600E-05
   22    0 3.000E-04-3.600E-05
   23    1-3.000E-04-7.200E-05
   33    0 3.000E-04-7.200E-05
   34    1-3.000E-04-1.080E-04
   44    0 3.000E-04-1.080E-04
   45    1-3.000E-04-1.440E-04
   55    0 3.000E-04-1.440E-04
   56    1-3.000E-04-1.800E-04
   66    0 3.000E-04-1.800E-04
   67    1-3.000E-04-2.160E-04
   77    0 3.000E-04-2.160E-04
   78    1-3.000E-04-2.520E-04
   88    0 3.000E-04-2.520E-04
   89    1-3.000E-04-2.880E-04
   99    0 3.000E-04-2.880E-04
  100    1-3.000E-04-3.240E-04
  110    0 3.000E-04-3.240E-04
  111    1-3.000E-04-3.600E-04
  121    0 3.000E-04-3.600E-04

elem
    1    1   12   13    2    1    1
   10    1   21   22   11   10    0
   11    1   23   24   13   12    1
   20    1   32   33   22   21    0
   21    1   34   35   24   23    1
   30    1   43   44   33   32    0
   31    1   45   46   35   34    1
   40    1   54   55   44   43    0
   41    1   56   57   46   45    1
   50    1   65   66   55   54    0
   51    2   67   68   57   56    1
```

```
   60     2   76   77   66   65     0
   61     2   78   79   68   67     1
   70     2   87   88   77   76     0
   71     2   89   90   79   78     1
   80     2   98   99   88   87     0
   81     2  100  101   90   89     1
   90     2  109  110   99   98     0
   91     2  111  112  101  100     1
  100     2  120  121  110  109     0

mate
    1     3| material number, element type number
          1| flag for time stepping (0 for no)
 0.667E+00| theta factor in transient algorithm
          1| degree of freedom number for displacements
 1.620E+11| elastic modulus
 2.000E+03| density
 4.960E+09| shear modulus
  0.27E+00| poisson's ratio
          3| degree of freedom number for temperature
  0.95E+00| thermal conductivity, y-direction
 18.00E+00| thermal conductivity, xz-direction
 1.160E+02| specific heat
 4.000E+02| thermomechanical dissipation factor
 3.000E+04| horn frequency (Hz)
          0| degree of freedom number for reaction (ndofc)
         1.| species diffusivity (d_diff)
         2.| kinetic order of reaction (x_m2)
         1.| rate constant preexponential factor (xk_0)
         1.| activation energy for reaction / gas constant (E_r)
         1.| heat of reaction (Q_r)
    2     3| material number, element type number
          1| flag for time stepping (0 for no)
 0.667E+00| theta factor in transient algorithm
          1| degree of freedom number for displacements
 1.694E+10| elastic modulus
 2.000E+03| density
 4.160E+10| shear modulus
 0.806E+00| poisson's ratio
          3| degree of freedom number for temperature
  0.95E+00| thermal conductivity, y-direction
 9.475E+00| thermal conductivity, xz-direction
 1.160E+02| specific heat
 4.000E+02| thermomechanical dissipation factor
 3.000E+04| horn frequency (Hz)
          0| degree of freedom number for reaction (ndofc)
         1.| species diffusivity (d_diff)
         2.| kinetic order of reaction (x_m2)
         1.| rate constant preexponential factor (xk_0)
         1.| activation energy for reaction / gas constant (E_r)
         1.| heat of reaction (Q_r)

boun
    6     0    1    1    0    0
  111     1   -1   -1   -1    0
  121     0    1    1    1    0
```

```
forc
    6    0 -13.8E-06 -8.00E-06     0.
  111    1   0.        0.        23.
  121    0   0.        0.        23.

end
macr
init
ltim      1.e-2  7.
disp
loop         18
ltim
form
tang
solv
disp
stre
next
dt          1.0
loop          8
time
form
tang
solv
disp
stre
next
end
    1  121    3     23.

stop
```

Appendix C UTL Code Listing

The codes listed below implements the finite element algorithm described in Chapter 2 and is the one used to generate the results shown in Chapter 4. The program is written in Fortran, and separated into a number of files denoted by ".for" or ".f" extensions.

The subroutine **elmt03.for** is the two dimensional loading and heat transfer element to model the processing of composite materials. It solves the equations governing the thermal-mechanical coupled transient problem. The subroutine **dma.for** is the code modeling the viscoelastic heat generation.

The main program is located in "**UTL.for**". Together with the attached subroutines **pcontr.for**, **pmacr.for**, **pmesh.for**, they initialize the computational domain, set up the geometry, get user inputs, and call macro solution module for establishing solution algorithm. Besides the essential procedures related directly to the implementation of UTL, a large number of small add-on subroutines have been implemented in the finite element package. Please refer to the Zienkiewicz text (1) for more details.

```
      subroutine elmt03(d,ul,xl,ix,tl,s,p,ndf,ndm,nst,isw)
c
c     two dimensional loading and heat transfer element
c     for UTL
c
      implicit real*8(a-h,o-z)
      common /cdata/  o,head(20),numnp,numel,nummat,nen,neq,ipr
      common /eldata/ dm,n,ma,mot,iel,nel
      common /tdata/  time,dt,c1,c2,c3,c4,c5
      common /movedata/ndoft,imax,jmax,xmax,xmin,ymax,ymin,Vhorn
      dimension d(30),ul(ndf,4),xl(ndm,4),ix(4),tl(4),
     1   s(nst,nst),p(nst),shp(3,9),sg(9),tg(9),wg(9),eps(5),sig(3),
     2   v(2),dv(2,2),xx(2),tau(3),dltee(2),dlcon(2),stress(3)
      equivalence (eps(4),S_energy),(eps(5),Q)
      real nu_xz, nu_zx

      go to (1,2,3,3,2,3), isw
c
c***********************************************************************
c
c     input/output material properties
c
c        allocation of material constants:
c
c        d(1)  -
c        d(2)  -
c        d(3)  - flag for time stepping (0 for no) (itime)
c        d(4)  - theta factor in transient algorithm (theta
c
c        d(5)  - degree of freedom number for displacements (ndofu)
c        d(6)  -
c        d(7)  -
c        d(8)  - bulk modulus (xk_bulk)
c        d(9)  - density (rho)
c        d(10) - shear modulus (G_shear)
c        d(11) -
c        d(12) -
c        d(13) -
c        d(14) -
c
c        d(15) - degree of freedom number for temperature (ndoft)
c        d(16) - y-direction thermal conductivity (cond_y)
c        d(17) - x&z-direction thermal conductivity (cond_xz)
c        d(18) - specific heat (c)
c
c        d(19) - degree of freedom number for reaction (ndofc)
c        d(20) -
c        d(21) - species diffusivity (d_diff)
c        d(22) - kinetic order of reaction (x_m2)
```

```
c        d(23) - rate constant preexponential factor (xk_0)
c        d(24) - activation energy for reaction / gas constant (E_r)
c        d(25) - heat of reaction (Q_r)
c        d(26) -
c        d(27) -
c        d(29) - horn frequency (freq, Hz)
c
c
 1010 format (i10)
 1020 format (g10.0)
c
    1 read (5,1010) itime
      read (5,1020) theta
      read (5,1010) ndofu
!      read (5,1020) xk_bulk,rho,G_shear
      read (5,1020) E_x,rho,G_shear
      read (5,1020) nu_xz                ! read nu_xz
      read (5,1010) ndoft
!      read (5,1020) cond_y,cond_xz,c,dissip
      read (5,1020) cond_y,cond_xz,c
      read (5,1020) freq
      read (5,1010) ndofc
      read (5,1020) d_diff
      read (5,1020) x_m2
      read (5,1020) xk_0
      read (5,1020) E_r
      read (5,1020) Q_r

      d(3)=itime
      d(4)=theta
      d(5)=ndofu
!      d(8)=xk_bulk
      d(8)=E_x
      d(9)=rho
      d(10)=G_shear
      d(11)=nu_xz                ! nu_xz
      d(15)=ndoft

c
      d(16)=cond_y
      d(17)=cond_xz
      d(18)=c
!      d(27)=dissip
      d(19)=ndofc
      d(21)=d_diff
      d(22)=x_m2
      d(23)=xk_0
      d(24)=E_r
      d(25)=Q_r

      d(29)=freq
c
      write (6,1100) itime,theta
 1100 format (/5x,'UTL element',
     *       /10x,'flag for time stepping (0 for no) =',i2,
     *       /10x,'transient algorithm theta value =',g12.4)
c
```

```
      write (6,1110) ndofu
 1110 format (  7x,'displacement parameters:',
     1        /10x,'displacement degree of freedom =',i2)
!      write (6,1120) xk_bulk,rho,G_shear
      write (6,1120) E_x,rho,G_shear
 1120 format (/10x,'bulk modulus =',g12.4,
     1        /10x,'density =',g12.4,
     2        /10x,'shear modulus =',g12.4)
c
!      write (6,1130) ndoft,cond_y,cond_xz,c,dissip,freq
      write (6,1130) ndoft,cond_y,cond_xz,c,freq
 1130 format (  7x,'thermal parameters:',
     *        /10x,'temperature degree of freedom =',i2,
     *        /10x,'y-conductivity =',g12.4,
     *        /10x,'xz-conductivity =',g12.4,
     *        /10x,'specific heat =',g12.4,
!     *         /10x,'dissipation factor =',g12.4,
     *        /10x,'horn frequency =',g12.4)

      write (6,1140) ndofc,d_diff,x_m2,xk_0,E_r,Q_r
 1140 format (  7x,'reaction parameters '
     *        /10x,'reaction degree of freedom =',i2,
     *        /10x,'species diffusivity =',g12.4,
     *        /10x,'kinetic order =',g12.4,
     *        /10x,'preexponential constant =',g12.4,
     *        /10x,'reaction activation energy/R =',g12.4
     *        /10x,'heat of reaction =',g12.4)

      lint=0
      return
c
c-----------------------------------------------------------------------
c
c     immediate return for isw = 2 or 5  (chec or lmas)
c
    2 return
c
c*****************************************************************
c*****************************************************************
c
c     form element stiffness matrices and load vectors
c
  3   lreg= 2
      lcont=2
      itime=d(3)
      if (itime.eq.0) dt=1.d0
      theta=1.d0
      if (itime.ne.0) theta=d(4)
      ndofu=d(5)
 !     xk_bulk=d(8)
      E_x=d(8)
      rho=d(9)
      G_shear=d(10)
      nu_xz=d(11)           ! nu_xz
      ndoft=d(15)
      cond_y=d(16)
      cond_xz=d(17)
```

```
      c=d(18)
!      dissip=d(27)
      ndofc=d(19)
      d_diff=d(21)
      x_m2=d(22)
      xk_0=d(23)
      E_r=d(24)
      Q_r=d(25)
      freq=d(29)
c**********************************************************************
c     loop over integration stations
c
 3140 if (lreg*lreg.ne.lint) call pgauss (lreg,lint,sg,tg,wg)
      do 6170 l=1,lint
c
      call shape (sg(l),tg(l),xl,shp,xsj,ndm,nel,ix,.false.)
      wgt=xsj*wg(l)
c
c----------------------------------------------------------------------
c
c     compute present values and gradients
c
      t=0.d0
      con=0.d0
      do 3160 i=1,2
         xx(i)=0.d0
         v(i)=0.d0
         dltee(i)=0.d0
         dlcon(i)=0.d0
         do 3150 j=1,2
 3150    dv(i,j)=0.d0
 3160 continue
c
      do 3190 k=1,nel
         if (ndoft.ne.0) t  =t  +shp(3,k)*ul(ndoft,k)
         if (ndofc.ne.0) con=con+shp(3,k)*ul(ndofc,k)
         do 3180 i=1,2
            xx(i)=xx(i)+shp(3,k)*xl(i,k)
            if (ndofu.eq.0) go to 3175
               v(i)=v(i)+shp(3,k)*ul(ndofu+i-1,k)
               do 3170 j=1,2
 3170          dv(i,j)=dv(i,j)+shp(j,k)*ul(ndofu+i-1,k)
 3175       if (ndoft.ne.0) dltee(i)=dltee(i)+shp(i,k)*ul(ndoft,k)
            if (ndofc.ne.0) dlcon(i)=dlcon(i)+shp(i,k)*ul(ndofc,k)
 3180    continue
 3190 continue

      eps(1)=dv(1,1)    !strains
      eps(2)=dv(2,2)
      eps(3)=dv(1,2)+dv(2,1)

      ! get modulus and dissipation from dma model
      call dma(freq,T,E_y,dissip)
c
      ! get stiffness matrix D using anisotropic derivation
      G_xz=G_shear
      G_xy=E_y/(2.*(1+nu_xy))
```

```
      nu_xy=.05
      nu_yx=nu_xy*E_y/E_x
      nu_zx=nu_xz*E_y/E_x
      D11=E_x*(1-nu_yx*nu_zx)/((1+nu_zx)*(1-nu_zx-2*nu_yx*nu_zx))
      D12=E_y*nu_zx/(1-nu_zx-2*nu_yx*nu_zx)
      D22=E_y*(1-nu_zx)/(1-nu_zx-2*nu_yx*nu_zx)
      D33=G_xy
c
!      call get_DD(E_x,E_y,G_shear,nu_xz,D11,D12,D22,D33)  !anisotropic
stiffness
c
      ! use equivalent strain for dissipation?
!     sig_eq=dsqrt(.5*((sig(1)-sig(2))**2+sig(1)**2+sig(2)**2
!     1       +6.*sig(3)**2))
c     Q=dissip*eps_eq**2
c
c-----------------------------------------------------------------------
c
c     fill out stiffness matrix (upper triangle)
c
 3205 if (isw.ne.3) go to 6
      theta=1.d0
      if (itime.ne.0) theta=d(4)
c
      k1=1
      do 3250 k=1,nel
cc
         j1=1
         do 3240 j=1,k
c

c           displacement contributions
c
            if (ndofu.eq.0) go to 3210

              u11=shp(1,j)*D11*shp(1,k)+shp(2,j)*D33*shp(2,k)
              u12=shp(1,j)*D12*shp(2,k)+shp(2,j)*D33*shp(1,k)
              u21=shp(2,j)*D12*shp(1,k)+shp(1,j)*D33*shp(2,k)
              u22=shp(2,j)*D22*shp(2,k)+shp(1,j)*D33*shp(1,k)

            jj=j1+ndofu-1
            kk=k1+ndofu-1
            s(jj  ,kk  )=s(jj  ,kk  )+u11*wgt
            s(jj  ,kk+1)=s(jj  ,kk+1)+u12*wgt
            s(jj+1,kk  )=s(jj+1,kk  )+u21*wgt
            s(jj+1,kk+1)=s(jj+1,kk+1)+u22*wgt
c
c           thermal contribution
c
 3210       if (ndoft.eq.0) go to 3240
            c11=0.d0
            if (itime.ne.0) c11=shp(3,j)*shp(3,k)*rho*c
            t11 = cond_xz*shp(1,j)*shp(1,k) + cond_y*shp(2,j)*shp(2,k)
            jj=j1+ndoft-1
            kk=k1+ndoft-1
            s(jj,kk)=s(jj,kk)+(t11*theta+c11/dt)*wgt
```

```
c           conversion contribution
c
 3220       if (ndofc.eq.0) go to 3240
            if (itime.ne.0) c11=c01
            cc11=s1*d_diff
            jj=j1+ndofc-1
            kk=k1+ndofc-1
            s(jj,kk)=s(jj,kk)+(cc11*theta+c11/dt)*wgt
c
c
 3240    j1=j1+ndf
 3250 k1=k1+ndf
      go to 6170
c
c---------------------------------------------------------------------
c
c     compute stresses, print strains
c
    6 if (ndofu.eq.0) go to 6040
      sig(1)=D11*eps(1)+D12*eps(2) !compute stresses from strains
      sig(2)=D12*eps(1)+D22*eps(2)
      sig(3)=D33*eps(3)
!     S_energy=.5*(sig(1)*eps(1)+sig(2)*eps(2)+sig(3)*eps(3))
      S_energy=.5*DABS(sig(2)*eps(2)+sig(3)*eps(3))
      Q=freq*S_energy*dissip

c
c      eps_eq=(sig(1)*eps(1)+sig(2)*eps(2)+sig(3)*eps(3))/E_real
c     Q=dissip*eps_eq

      if (isw.eq.6) go to 6040
c
      mot=mot-1
      if (mot.gt.0) go to 6025
      write (6,6010) o,head,time
 6010 format (a1,20a4,//5x,'element stresses at time',g12.4,
     1   //1x,'elmt matl',6x,'x-coord',6x,'y-coord',4x,'eps_x',5x,
     2   'eps-y',7x,'eps-xy',7x,'eps_eq',7x,'Q'/)
      mot=50
 6025 write (6,6030) n,ma,xx,eps
 6030 format (2i5,8g13.4)
      write (7,6035) n,xx,eps
 6035 format (i5,5g13.4,/31x,3g13.4)
      go to 6170
c
c---------------------------------------------------------------------
c
c     fill out unbalanced force vector
c
 6040 continue
      j1=1
         k=1
 6050    continue
c
c        displacement contribution
c
         if (ndofu.eq.0) go to 6100
```

```
         u1=shp(1,k)*sig(1)+shp(2,k)*sig(3)
         u2=shp(2,k)*sig(2)+shp(1,k)*sig(3)

         jj=j1+ndofu-1
         p(jj  )=p(jj  )-u1*wgt
         p(jj+1)=p(jj+1)-u2*wgt
c
c        thermal contributions (no reaction heat considered yet)
c
 6100    if (ndoft.eq.0) go to 6150
 6120    t1=Q*shp(3,k)
         t2=cond_xz*shp(1,k)*dltee(1)+cond_y*shp(2,k)*dltee(2)
         jj=j1+ndoft-1
         p(jj)=p(jj)+(t1-t2)*wgt     !!! minus sign on t1???
c
c        conversion contributions
c        assume reaction consumptive, subtract cc1 term
c
 6130    if (ndofc.eq.0) go to 6150
         rate=xk_0*dexp(-E_r/(T+273.))*(1-con)**(3-x_m2)*(con**x_m2)
         cc1=rate*shp(3,k)
         cc2=(shp(1,k)*dlcon(1)+shp(2,k)*dlcon(2))*d_diff
         q=q+Q_r*rate
         jj=j1+ndofc-1
         p(jj)=p(jj)+(-cc1-cc2)*wgt
c
c
 6150    j1=j1+ndf
 6160 k=k+1
      if (k.le.nel) goto 6050
c
c-----------------------------------------------------------------------
c
c     end loop on integration stations
 6170 continue
c
      if (isw.eq.4) return
      if (isw.eq.6) go to 6200
c
c     form lower triangular array by symmetry
c
      do 6180 j=2,nst
      jm1=j-1
      do 6180 k=1,jm1
 6180 s(j,k)=s(k,j)

 6200 return

      end
```

```
subroutine dma(freq,T,E_y,dissip)

! compute modulus and dissipation for given frequency and temperature
! 8552 epoxy - Zukas data, Weichert model

implicit real*8 (a-h,o-z)
real*8      kj
dimension kj(7),tauj(7)
data kj
/1.11E+06,5.56E+06,1.03E+07,2.50E+07,8.42E+07,2.10E+08,2.87E+07/
data tauj/8.87E-11,8.87E-12,8.87E-13,8.87E-14,8.87E-15,8.87E-16,8.87E-
17/

pi=3.14159
E_v= 69.1*1000      !activation energy, J/mol
R=8.314             !gas constant, J/mol-K
omega=2.*pi*freq  !convert from Hz to rad/s

E_real=1.18E+08
E_loss=0.
exp_T=dexp(E_v/(R*(T+273)))

weichert:do j=1,7   !sum over arms of model

  tau=tauj(j)*exp_T
  E1_j= kj(j)*(omega**2)*(tau**2)/(1+(omega**2)*(tau**2))
  E2_j= kj(j)*omega*tau/(1+(omega**2)*(tau**2))
  E_real=E_real+E1_j
  E_loss=E_loss+E2_j

end do weichert

E_y=E_real
dissip=2.*pi*E_loss/E_real

return
end
```

Appendix D Post-Processor Code Listing

The codes listed below implements post-processing part to plot the output of UTL.for. The program is written in Fortran, and separated into a number of files denoted by ".for" or ".f" extensions.

The main program is located in "**POST.for**". Together with the attached subroutines **discon.for**, **strscon.for**, **strs.for**, and **contr.for**, they set up the geometry, get user inputs, and plot the mesh, the contours plots of displacements and strains. Besides the essential procedures related directly to the implementation of UTL, a large number of small add-on subroutines have been implemented in the post-processing package. Please refer to the Zienkiewicz text (1) for more details.

```
subroutine dispcon

      use msflib
      include 'comvariable.h'

c      type (xycoord) xy
      type (rccoord) curpos
c      character(80) title
c     character(1) key
c     character(1) key
c
c     D - plot displacement contours
c
      msg='enter dof number, press return'
      call prompt1 (msg)
      msg=' '
      call prompt2 (msg)

      CALL SETTEXTPOSITION (INT2(3), INT2(8), curpos)
      RESULT = SETTEXTCOLORRGB(#00FF00)        ! Green
c     call moveto( INT2(100), INT2(750), xy)
      numfonts = INITIALIZEFONTS ( )
      fontnum = SETFONT ('t''Arial''h14pi')
      read (5,*) ndof
c
c      color=ltcyan
      if ( ndof.lt.3) then
      call contr (ul(1,ndof))
      call boun
      endif
c      else

c10   call getop(key)

c        if (key.eq.'c') then   ! clear screen and plotfile
c
c        BKCOLOR = SETBKCOLORRGB(#FFFFFF)
c         CALL CLEARSCREEN ($GCLEARCREEN)

c        numfonts = INITIALIZEFONTS ( )
c        fontnum = SETFONT ('t''Arial''h24w10i')

c        CALL moveto(INT2(1),INT2(1),xy)
c         oldcolor=SETCOLORRGB(#FF0000)      ! Blue
c         CALL OUTGTEXT (title)

c        call setlinestyle( INT2(#FFFF))        ! Solid
c        oldcolor = SETCOLORRGB(#0000FF)      ! Red
c        dummy=rectangle( $gborder, 1, 30, 1278, 700 )
c            msg='options:
Boun,Clear,Disp,Elnum,Mesh,Nodenum,Quit,blacKboun,Wr
c     $ite'
c       call prompt1 (msg)
c       msg = ' '
c       call prompt2 (msg)
c        endif
c     goto 10
```

```
        return
        end
-
```

```
      subroutine strscon

      use msflib

      include 'comvariable.h'
      common /stres/isw

      type(xycoord) xy
c
c     S - plot stress contours
c
      isw=8
      msg='enter component number, press return'
      call prompt1 (msg)
      msg=' '
      call prompt2 (msg)
      call moveto( INT2(23), INT2(6), xy)
c
      color=ltred
      read (*,*) kcomp
c
c     write (7,8040)
c8040 format (1x,'enter material set number')
c     read (5,*) mat
      mat=0
 10   continue
      mat=mat+1
c     write (8,*) 'for mat, stress comp. = ',mat,kcomp
      if (mat.gt.nummat) then
         call boun
         isw=0
         return
      endif
c
      if (kcomp.eq.10) go to 8200
      if (kcomp.eq.11) go to 8300
      if (kcomp.eq.12) go to 8400
      if (kcomp.gt.6) go to 8050
c
         call strs (kcomp)
         go to 900
c
 8050 call strs (4)
      do 8060 i=1,numnp
 8060 str(i)=stress(i,1)
      call strs (5)
```

```
      do 8070 i=1,numnp
         p1=str(i)
         p2=stress(i,1)
         if (kcomp.eq.7) stress(i,1)=p1-p2
         if (kcomp.eq.8) stress(i,1)=(1./3.)*sqrt((p1-p2)*(p1-p2)
     1                                  +(p1*p1)+(p2*p2))
         if (kcomp.eq.9) stress(i,1)=p1+p2
 8070 continue
c8080 call contr (stress)
 8080 go to 900
c
c     remove comments for output to line printer
c
c     write (8,8150) title,mat,kcomp
c8150 format (1h1,/1x,20a4,
c    1   //5x,'averaged nodal stresses for material set',i2,
c    2   //6x,'node',4x,'x-coord',8x,'y-coord',8x,i1,'-stress'/)
c
c     do 8170 i=1,numnp
c        xx=(x(i)+delx)/scale
c        yy=(y(i)+dely)/scale
c        write (8,8160) i,xx,yy,stress(i,1)
c8160    format (6x,i3,1x,3g15.4)
c8170 continue
c
c     go to 900
c
c     routines for elmt03 fluid element
c     components of stress:
c        1. vorticity
c        2. pressure
c        3. tau-xx
c        4. tau-yy
c        5. tau-xy
c        6. tau-theta
c
c
c     fluid distortional energy (sum tau^2)
c
 8200 call strs (3)
      do 8210 i=1,numnp
 8210 str(i)=(stress(i,1))**2
c
      call strs (4)
      do 8220 i=1,numnp
 8220 str(i)=str(i)+(stress(i,1))**2
c
      call strs (5)
      do 8230 i=1,numnp
 8230 stress(i,1)=str(i)+(stress(i,1))**2
c
c     call contr (stress)
      go to 900
c
c     fluid principal stress (kcomp=11)
c
 8300 call strs(2)
```

```
      do 8310 i=1,numnp
 8310 str(i)=stress(i,1)
c
      call strs(3)
      do 8320 i=1,numnp
 8320 sxx(i)=stress(i,1)
c
      call strs(4)
      do 8330 i=1,numnp
 8330 syy(i)=stress(i,1)
c
      call strs(5)
      do 8340 i=1,numnp
 8340 sxy(i)=stress(i,1)
c
      do 8350 i=1,numnp
         x1=(sxx(i)+syy(i))/2.d0
         x2=(sxx(i)-syy(i))/2.d0
         x3=sxy(i)
         root=sqrt(x2*x2+x3*x3)
         stress(i,1)=str(i)+x1+root
 8350 continue
      go to 900

c     von Mises stress for axisymmetric element mesh

8400  call strs(4)
      do 8410 i=1,numnp
8410  sxx(i)=stress(i,1)

      call strs(5)
      do 8420 i=1,numnp
8420  syy(i)=stress(i,1)

      call strs(6)
      do 8430 i=1,numnp
8430  sxy(i)=stress(i,1)

      do 8440 i=1,numnp
         x1=(sxx(i)-syy(i))**2
         x2=(sxx(i)-sxy(i))**2
         x3=(syy(i)-sxy(i))**2
         stress(i,1)=(1./3.)*sqrt(x1+x2+x3)
8440  continue
      go to 900
c
  900 continue
      call contr (stress)
      go to 10
      end
```